Title: Astrocyte Contribution to Brain State-Dependent Neurovascular Coupling

Authors: Jakob Akbar Stelzner[1]*, Aske Krogsgaard[1]*, Gabriele Kulkoviene[1,2,3], Leonora Sperling[1], Barbara Lykke Lind[1,°]

Affiliations:

[1]Department of Neuroscience, Faculty of Health Sciences, University of Copenhagen, DK-2200 Copenhagen N, Denmark

[2]Laboratory of Pharmaceutical Sciences, Institute of Pharmaceutical Technologies, Lithuanian University of Health Sciences, LT-50166 Kaunas, Lithuania

[3]Department of Drug Chemistry, Pharmacy Faculty, Lithuanian University of Health Sciences, LT-50166, Kaunas, Lithuania.

*Shared first authors.

°corresponding author; +45 61777970, barbarall@sund.ku.dk , https://orcid.org/0000-0003-0027-5226

Abstract

The process of neurovascular coupling (NVC) is the regulation of sufficient and targeted blood flow during energy-consuming cerebral processes. Astrocyte participation in NVC has long been debated. The lack of clear answers is likely based on the diversity of astrocyte intracellular Ca2+ activities and the multitude of ways astrocytes may regulate cerebral blood flow. We focused our investigation on NVC responses to sensory input actively reached for by freely behaving mice. To do so, we studied the cellular and vascular activity in the sensory whisker barrel cortex of awake head-fixed mice and aligned this activity to the volitional whisking events. We compared the NVC initiated by the whisking event in the resting mouse to the whisking evoked by the experimenter and the whisking prior to locomotion. We did this comparison because astrocyte signaling is known to be sensitive to brain state transitions. In the NVC response to all three, we found that both neuronal and astrocytic activity corresponded to vascular activity. When we repeated this investigation after depletion of NA release from locus coeruleus projections, we identified that the three NVC responses did not equally depend on NA delivery or astrocytic activity. Though we found the expected effect on astrocytic Ca2+ surges, the whisking-dependent astrocytic Ca2+ activity was only moderately reduced by the reduced NA levels in the resting mouse and only in cells near the vessels. On the vascular side, we found that the dilation of the 1st order capillary to volitional whisking was much reduced. This suggests a disturbance in the precision regulation of the cerebral blood flow that may limit the appropriate delivery of blood to the region of activated neurons. Finally, this disturbance might partially account for the extended period of exploratory whisking prior to the initiation of locomotion that we saw in the NA-depleted mice. Our study reveals an astrocytic contribution to NVC in the natural shifts in the attention directed toward the sensory input received during volitional whisking.

Introduction

Neurovascular coupling (NVC) is the process that recruits additional local cerebral blood flow (CBF) to match the increased energy demands during local brain activation (Roy and Sherrington 1890). Over the years, several cell types have been identified to partake in this process, amongst them astrocytes, which are known to possess several, and even counteracting, regulatory mechanisms (Howarth, Mishra et al. 2021, Schaeffer and Iadecola 2021). With such an ambiguity of regulative mechanisms in the cells surrounding the brain vasculature, the question must be when each contributes. This is important to clarify as several CNS diseases present with a disruption in the NVC(Schaeffer and Iadecola 2021). We

know that the dynamics involved in cortical excitement in awake and freely behaving animals depend on the shifting activation of complex neuronal circuits (Petersen 2019) and on neuromodulator release patterns (Collins, Francis et al. 2023). Both systems depend on and contribute to the shifting brain states. There is a high diversity in NVC responses in different brain regions (Drew 2022). We propose that this diversity depends on the manner of neuronal excitation. And that the behavioral and brain state context of neuronal excitation influences which blood flow recruiting mechanisms are at work. If so, it would imply that additional energy substrates and oxygen are not provided through identical mechanisms during different cognitive tasks. Astrocytes are a cell type whose activity is acutely dependent on brain state (Bindocci, Savtchouk et al. 2017, Bojarskaite, Bjornstad et al. 2020, Krogsgaard, Sperling et al. 2023, Reitman, Tse et al. 2023). Its processes enwrap both synapses and the brain microvasculature(Mathiisen, Lehre et al. 2010, McCaslin, Chen et al. 2011), which makes them ideally situated for integrating information about synaptic activity and relaying this information to blood vessels. However, investigations into its contribution to NVC have reached different conclusions (Takano, Tian et al. 2006, Petzold, Albeanu et al. 2008, Nizar, Uhlirova et al. 2013, Bonder and McCarthy 2014, Institoris, Rosenegger et al. 2015, Lacroix, Toussay et al. 2015, Masamoto, Unekawa et al. 2015, Del Franco, Chiang et al. 2022). The uncertainty may be due to the behavioral context in which these studies have been conducted, the most prominent of which is during anesthesia. It is equally likely that it comes down to analysis strategy and hos astrocytic activation was identified. Astrocyte activation is measured by imaging methods; thus, it is not irrelevant how regions of activity and criteria for responses are defined. We and others have previously shown that astrocytic Ca2+ transients may occur on a fast timescale, very similar to Ca2+ transients in neurons and that these may be involved in recruitment during NVC (Winship, Plaa et al. 2007, Lind, Brazhe et al. 2013, Otsu, Couchman et al. 2015, Lind, Jessen et al. 2018). Other roles have been suggested for astrocytes in NVC, such as extending the late vasoconstrictive phase of (Mulligan and MacVicar 2004, Metea and Newman 2006, Gordon, Choi et al. 2008, Girouard, Bonev et al. 2010) or amplifying the response (Gu, Chen et al. 2018, Institoris, Vandal et al. 2022). It has also been suggested that the astrocytic contribution to NVC is capillary-specific (Biesecker and Srienc 2015, Mishra, Reynolds et al. 2016). Hence, we focused our investigation on the vascular inflow tract where a 1st order capillary branch from the penetrating arteriole (PA). Dilation of either of these two parts of the vascular inflow tract delivers additional blood to the cortical tissue downstream from this branchpoint. PA expansions provide a larger inflow to deeper cortical layers, whereas a capillary dilation creates a more local blood flow increase. Regulation of the dilations in the whisker barrel cortex is expected to match the area of neuronal excitation created by sensory input through whisker deflections. Hence, this point

in the vascular tree is a key regulation point in the delivery of freshly oxygenated blood to the cerebral tissue (Grubb, Cai et al. 2020, Hartmann, Coelho-Santos et al. 2022). We investigated the astrocytic calcium involvement in CBF regulation in the somatosensory barrel cortex during volitional whisking in awake mice. Up to now, most studies of NVC in whisker barrel cortex use a forced stimulation protocol (Ding, O'Donnell et al. 2013, Stobart, Ferrari et al. 2018, Tran, Peringod et al. 2018, Sharma, Gordon et al. 2020). However, this approach only targets one pattern of cognitive involvement of the mouse, namely the unsuspected excitation of the sensory cortex. Whisking deflection activates the whisker barrel cortex through thalamocortical input (Petersen 2019), in combination with noradrenaline (NA) release by projections from the locus coeruleus (LC) (Kim, Jung et al. 2016, Collins, Francis et al. 2023). It has been shown that the release of NA from LC alone can trigger a cortical blood flow response (Toussay, Basu et al. 2013, Lecrux, Sandoe et al. 2017). The degree of NA contribution to NVC should thus depend on whether the whisking is volitional surveillance or due to a change in the alertness of the animal(Shimaoka, Harris et al. 2018). We compared NVC responses to volitional whisking during rest, locomotion, and evoked stimulation. All three types of whisker deflection are associated with increased activity in noradrenaline (NA), releasing projections from locus coeruleus (LC)(Collins, Francis et al. 2023). Only one other study has looked at the blood flow responses to volitional whisking during rest (Winder, Echagarruga et al. 2017), while several have considered the whisking associated with locomotion(Tran, Peringod et al. 2018, Eyre, Shaw et al. 2022). Running is strongly associated with whisking(Sofroniew, Cohen et al. 2014) and evokes noradrenaline-dependent astrocytic calcium responses (Ding, O'Donnell et al. 2013). We, therefore, speculated that astrocyte contribution to NVC was not equal during rest versus locomotion. And that this was dependent on cortical NA dynamics.

We found that regardless of whisker deflection context, an NVC response in the barrel cortex always entailed a neuronal excitation, shortly followed by an astrocytic Ca2+ response and then a dilation of the neighboring blood vessels. After dilation had peaked, a second astrocytic response could be observed. The size and location of the early astrocytic Ca2+ activity correlated with the size and location of neuronal excitation, independent of whether the whisking was evoked or volitional, during rest or during running. During rest, neuronal excitation and vessel dilations correlated with the length of the volitional whisking, indicating that NVC correlates well with the amount of sensory input. The increased neuronal excitation was mirrored in dilation size. In contrast, during locomotion, blood vessel expansion no longer matched the neuronal excitation. The timing of the increased astrocytic Ca2+ activity during locomotion excluded that it could explain this mismatch. We used DSP-4, a neurotoxin that transiently eliminates the noradrenergic projections from locus coeruleus(Slezak, Kandler et al. 2019, Renden, Institoris et al.

2024), to investigate the NA contribution to NVC. The effect of this treatment on the three different whisking-related NVC responses was dissimilar. In the evoked responses, the lack of NA release reduced neuronal responses furthest from the vasculature but did not otherwise affect the astrocytes or the NVC responses. In volitional whisking during rest, the NA-depletion only affected astrocytic Ca2+ responses and 1st order capillary dilations. This result indicates a critical contribution from astrocytes to the laminar and localized blood flow regulation in the context of volitional and expected sensory input from the whisker pad. Remarkably, this reduction in whisking-associated astrocytic and local blood flow activation appeared to delay the period from the onset of volitional whisking to the onset of locomotion. Once locomotion was initiated, neuronal, blood vessel and early astrocytic activity were no longer inhibited by the lack of NA release from LC. These findings show that it is possible to identify NVC-relevant astrocytic activity, which is both temporally and spatially recurrent, though not to the same degree as in neurons. And that NVC responses during whisker pad activity depend on NA release and astrocytic activity when the whisker deflection is volitional.

Results

Self-initiated whisking events trigger NVC responses, which depend on whisking duration.

We used awake, behaving mice to study intracellular calcium activity and hemodynamic responses during natural spontaneous whisking (Figure 1A). Data was recorded with two-photon microscopy imaging (2PM) from layer II/III of the whisker barrel cortex of adult mice. Blood flow regulation was evaluated by staining the lumen of the vasculature with a Texas Red dextran injected i.v. prior to the imaging. The lumen staining revealed dilations and constrictions of the blood vessels. Viral vectors were injected to express Ca^{2+} indicators to specific cell types. During imaging, the head was fixed beneath the objective, but the mouse was free to move within an airlifted mobile homecage, which tracked the animals' movements (Figure 1A). The benefit of using the whisker barrel cortex to study neurovascular coupling (NVC) responses was that we had a visual cue to when sensory input flowed via the thalamus to the cortex. We got this by monitoring the snout of the mouse with an IR camera during the two-photon imaging (Figure 1A) and then employ a motion detection algorithm to detect whisking events (Sup. Figure S1). Relating these data with the output from the sensor in the homecage, we could detect whether the mouse was either resting or running as it moved its whiskers. Locomotion was always associated with whisking, but the resting mouse also regularly moved its whiskers, with a mode of every 2 seconds (Sup. Figure S2). The whisking periods in the resting animal lasted on average 0.96s±0.046 s (Sup. Figure S2), of which 8% were of a >2 s duration (22%more than 1s). We then investigated how well

these volitional whisking events recruited an NVC response in the receiving whisker barrel cortex. Our imaging was focused on the first regulation point in the vascular inflow tract. Here we quantified the cross area of both the penetrating arterioles and the 1st order capillary branching from it (Grubb, Cai et al. 2020, Hartmann, Coelho-Santos et al. 2022) (Figure 1B). We found frequent changes in vessel lumen at this point in the vascular tree, and they appeared to correlate to the volitional whisking activity of the spontaneously behaving mouse. To quantify this volitionally triggered neurovascular coupling, we aligned spontaneously occurring whisking events with the changes in the vessel area (Figure 1C). When sorting whisking events at ½ second intervals, we found that the onset of natural whisking in stationary mice was strongly associated with vasodilation of both the PA and 1st order capillary and that even the shortest whisking event would cause a dilation (Figure 1D and F). As would be expected, longer whisking events evoked larger vasodilations of PA and 1st order capillary (Figure 1E and G) (Pearson correlation amplitude PA: R = 0.98, p = 0.0006 and AUC R = 0.97, p = 0.0012, N=21 FOV in 16 mice, 1st order cap.: R = 0.94, p = 0.0049 and AUC R = 0.84, p = 0.0038 N= 10 FOV in 7 mice).

Self-initiated whisking events trigger spatially recurrent astrocytic Ca2+ activities that rise before the dilations of the blood vessels and coincide with neuronal activation.

To visualize astrocytic activity during the volitional NVC response, we used GCaMP6f under the gfaABC1D promotor. This Ca^{2+} indicator was tethered to the cell membrane to better visualize activity in small processes(Shigetomi, Bushong et al. 2013). Given the current uncertainty with regard to astrocytic responses in the context of NVC, it was a strong priority that the intracellular Ca^{2+} changes were analyzed using an automated definition of the ROIs (region of activity) to minimize the risk of bias associated with manual ROI placement. Hence, we first turned to a custom-written automated event detector with a dynamic ROI definition similar to aQua(Wang, DelRosso et al. 2019, Krogsgaard, Sperling et al. 2023) (Supplemental figure S3). This method detected large and spatially heterogeneous dynamics in astrocyte Ca2+ activity (Supplemental Figure S4A). Similar astrocytic Ca2+ activity has often been described in awake mice(Bindocci, Savtchouk et al. 2017, Reitman, Tse et al. 2023). The average activity from these dynamic ROIs was ambiguously correlated to whisking activity (Supplemental Figure S4B and C), but a response did occur, which was significant compared to random timepoints (Supplemental Figure S4D). We suspected that the dynamic ROI detection method could be flawed towards selecting regions with the highest level of Ca2+ activity while not selecting smaller but recurrent dynamics. Since previous studies suggest that the larger astrocytic Ca2+ surges are not relevant for the recruitment of blood in neurovascular coupling(Institoris, Vandal et al. 2022), we developed an alternative method to define the

ROIs. This method was also automated but biased towards regions with spatially recurrent Ca2+ activity during neurovascular coupling events triggered by volitional whisking (Figure 1H, Supplementary Figure S5). We identified whisking-dependent ROIs by aligning the images in time relative to the peaks of the PA dilations occurring during the whisking (Figure 1H). This average revealed that some astrocytic activity rose during whisking prior to the dilation (Figure 1H). Thus, we focused our algorithm on detecting the spatial locations of this earliest astrocytic activity by selecting regions with a high level of activity preceding this dilation (Figure 1I, supplemental figure S5). These ROIs were then applied to detect Ca2+ activities during all imaging sessions of this specific FOV. Because of the large surges sometimes occurring in astrocytic Ca2+ levels, we normalized the signal from the activity-dependent ROIS to the seconds prior to each whisking event, not to the full 2min imaging sequence. When we then aligned the average astrocytic Ca2+ to whisking duration we found a correlation, though less strong than the vascular response (Pearson correlation R = 0.894, p = 0.0164, N= 21 FOV in 16 mice, Figure 1J and K). The astrocytic Ca2+ activity in these ROIS fell in two peaks, so that the Ca2+ activity rose significantly above baseline both prior to and after the dilation (T-test comparing to baseline Early Ca2+ max: p= 8.7*10-153 AUC: p=0.0033, Late Ca2+ max: p= 3.4*10-171AUC p=0.00092, N=989, 21 FOV 16 mice) (Figure 1L). These two peaks were strongest in the astrocytic ROIs closest to the PA (Supplemental Figure S6). The peaks in the average signal only reflected some degree of synchronicity, as we found that the astrocytic response to the individual whisking events showed heterogeneity in timing, modality, and even occurrence (Figure 1M, above). The timing of astrocytic responses matters as it decides whether this cell type can contribute to blood flow recruitment in NVC responses. The earlier peak could reflect the astrocytic response to synaptic activity during sensory-based excitation(Bindocci, Savtchouk et al. 2017, Arizono, Inavalli et al. 2020). To investigate how neurons responded to volitional whisking activity in naturally behaving animals, we evaluated neuronal activity using the synapsin promotor to obtain a general neuronal expression of the Ca2+ indicator GCaMP7. This indicator was virally introduced to the barrel cortex of another group of mice and then studied with the volitional NVC responses of similar vascular inflow tracts (Figure 1N). An imaging session of the spontaneous neuronal Ca2+ activity in the synGCamP7 mice showed high heterogeneity. Still, the average neuronal Ca2+ levels did change in correspondence with the volitional whisking events during rest and in the period when the mouse was running. To localize this signal, we identified regions of whisking-related activity by correlating to whisking onset (Supplemental Figure S7). This method revealed that most whisking-related neuronal activity appeared within ROIs with an area <1μm^2 (Supplemental Figure S7). Based on neurons' known anatomy and function, we classify them as synaptic structures. ROIs larger than 1μm^2 were considered

dendrites, whereas somas were manually selected. Average activity in all neuronal compartments correlated well with the volitional whisking activity (Supplemental Figure S7). Of the different groups of neuronal whisking-related ROIs, we found that the average response from synaptic ROIs in the proximity of the vessels had the best correlation with whisking duration (Pearson correlation R = 0.939, p = 0.00531, N=19 FOV in 7 mice Supplemental Figure S7 and Figure 1N-P). Similar to what was seen in the astrocytes, the neuronal activity during the individual volitional whisking events was also heterogeneous with regard to timing, modality, and occurrence (Figure 1M, below). This heterogeneity shows that other parameters besides the whisking define the strength of the neuronal excitation. It is likely that the variance in neuronal activation could explain some of the variance in astrocytic response. Another parameter that changes with whisking (Collins, Francis et al. 2023) and could affect astrocytic activity during volitional NVC responses would be an increase in extracellular NA. The changes in pupil size reflect the degree of systemic NA releases(Reitman, Tse et al. 2023). Thus, we investigated the pupil of a group of mice during the volitional whisker movements (Figure 1Q and supplemental figure S8). To investigate how much arousal affected the astrocytic responses to volitional whisking, we aligned the changing pupil size to the onset of whisking events (Figure 1R). This investigation revealed that there was indeed some change in the alertness and arousal state of the animal, even with the shortest whisking activities. The expected dilation was preceded by a constriction, likely because our definition of a whisking onset required a period of 0.5 sec without whisking (Figure 1R). This alignment reveals that the pupil was as equally enlarged by whisking as the lack of whisking constricted it and should be described as in sync with the whisking rather than as a response to the whisking. The size of the pupil dilations in sync with whisking did not correlate with whisking duration (Figure 1S, Pearson correlation R = 0.698, p = 0.1226, N=6 mice), though the dilations appear to be slightly larger to volitional whisking events longer than 1s. This is in accordance with the recent description of increased activation of NA positive projections from the locus coeruleus during volitional whiskings >1s duration(Collins, Francis et al. 2023). We must thus expect some degree of brain state shift in the context of our volitional NVC events(Turner, Gheres et al. 2023).

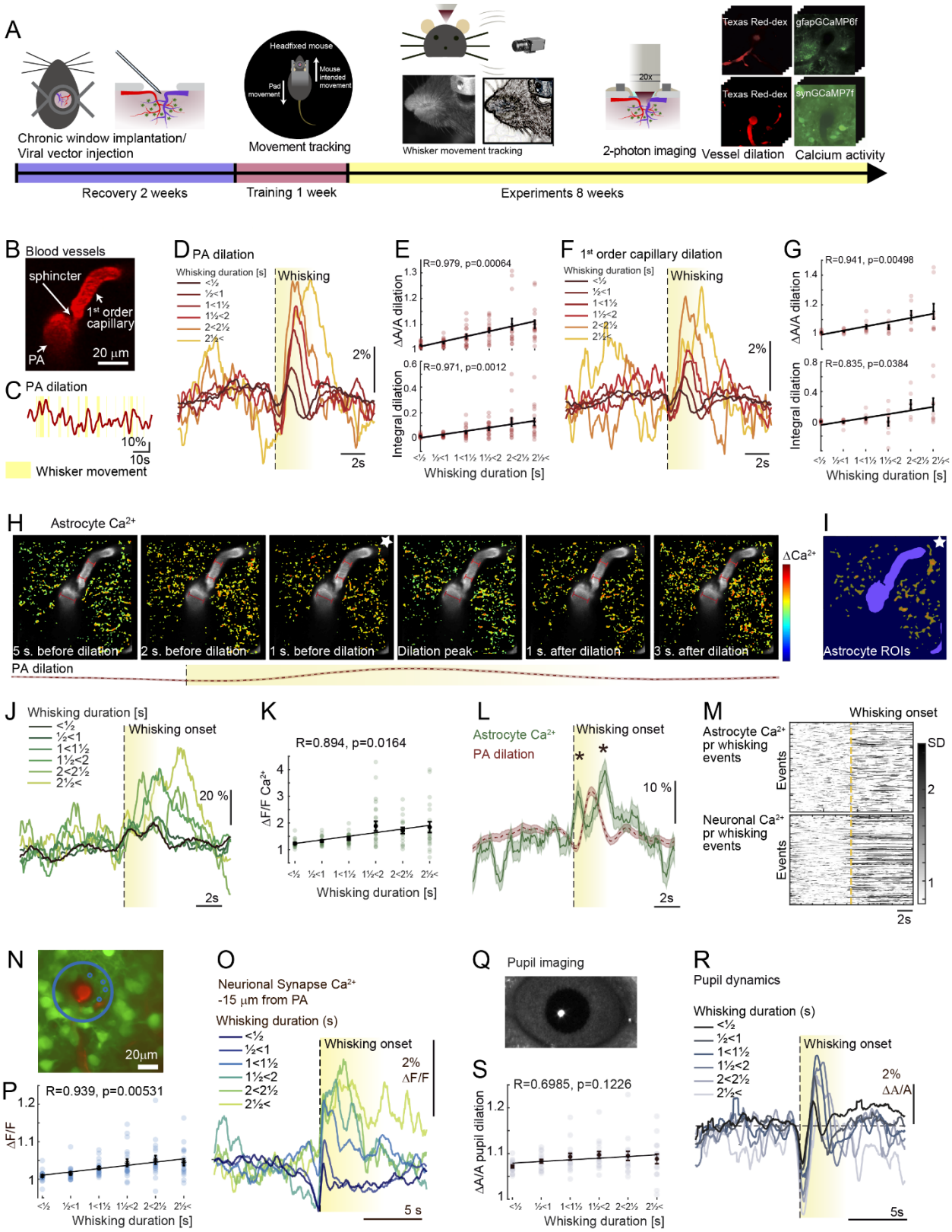
A
Chronic window implantation/
Viral vector injection
Headfixed mouse
Pad movement
Mouse intended movement
Movement tracking
Whisker movement tracking
20x
2-photon imaging
Texas Red-dex
gfapGCaMP6f
Texas Red-dex
synGCaMP7f
Vessel dilation
Calcium activity
Recovery 2 weeks
Training 1 week
Experiments 8 weeks
B Blood vessels
sphincter
1st order capillary
PA
20 µm
C PA dilation
10%
10s
Whisker movement
D PA dilation
Whisking duration [s]
<½
½<1
1<1½
1½<2
2<2½
2½<
Whisking
2%
2s
E
R=0.979, p=0.00064
ΔA/A dilation
R=0.971, p=0.0012
Integral dilation
Whisking duration [s]
F 1st order capillary dilation
Whisking duration [s]
Whisking
2%
2s
G
R=0.941, p=0.00498
ΔA/A dilation
R=0.835, p=0.0384
Integral dilation
Whisking duration [s]
H Astrocyte Ca2+
5 s. before dilation
2 s. before dilation
1 s. before dilation
Dilation peak
1 s. after dilation
3 s. after dilation
ΔCa2+
PA dilation
I
Astrocyte ROIs
J Whisking duration [s]
Whisking onset
20 %
2s
K
R=0.894, p=0.0164
ΔF/F Ca2+
Whisking duration [s]
L
Astrocyte Ca2+
PA dilation
Whisking onset
10 %
2s
M
Whisking onset
Astrocyte Ca2+ pr whisking events
Neuronal Ca2+ pr whisking events
Events
SD
2s
N
20µm
O
Neurional Synapse Ca2+
-15 µm from PA
Whisking duration (s)
Whisking onset
2%
ΔF/F
5 s
P
R=0.939, p=0.00531
ΔF/F
Whisking duration [s]
Q Pupil imaging
S
R=0.6985, p=0.1226
ΔA/A pupil dilation
Whisking duration [s]
R
Pupil dynamics
Whisking duration (s)
Whisking onset
2%
ΔA/A
5s

Figure text, figure 1 Self-initiated whisking events trigger neurovascular coupling responses that depend on whisking duration and spatially recurrent neuronal and astrocytic Ca2+ activities rise before the dilations.

A) Experimental setup and protocol. A viral vector was injected when the chronic window was implanted. After two weeks of recovery, mice were gradually habituated to experimental conditions. Locomotion events were extracted from the measurement of the movement of the mobile homecage. Whisker movement was monitored using a video camera and analyzed for natural whisking activity. Cellular calcium activity and vascular responses were measured using two-photon microscopy.

B) Texas Red-dextran loaded penetrating arteriole (PA) and 1st order capillary branching point in the layer II/III of whisker barrel cortex. A clear precapillary sphincter is visible.

C) Example traces of vasodilations overlaid with yellow shaded areas representing whisking.

D) Average vasodilation of PA to all volitional whisking events of increasing duration.

E) **Top:** Amplitude of PA vasodilations as a function of whisking event duration. Pearson correlation R = 0.98, p = 0.0006. **Bottom:** AUC of PA vasodilations as a function of whisking event duration. Pearson correlation R = 0.97, p = 0.0012. N= 20 FOV in 16 mice

F) Average vasodilation of 1st order capillary to all volitional whisking events of increasing duration.

G) **Top:** Amplitude of 1st order capillary vasodilations as a function of whisking event duration. Pearson correlation R = 0.94, p = 0.004. **Bottom:** AUC of vasodilations as a function of whisking event duration. Pearson correlation R = 0.84, p = 0.034. N= 10 FOV in 7 mice

H) 2-photon images from FOV 120µm below the cortical surface, aligned to dilation peak associated with volitional whisking (Outlined below). Dilation of both penetrating arteriole (PA) and 1st order capillary (white) and astrocytic Ca2+ increase before and after dilation peaks (pseudocolor). Ca2+ activity normalized to s.d. values per pixel over time shown in pseudocolor, overlayed greyscale image of vessels, red scalebar show dilation of both PA (dark red) and 1st order capillary (light red).

I) Mask of vessels (purple) and activity-dependent ROIs detecting astrocytic responses prior to dilation peak (Imaged marked with white star in H).

J) Astrocytic Ca2+ averaged from all activity-dependent ROIs during all volitional whisking events of increasing duration aligned to whisking onset.

K) The amplitude of astrocytic calcium responses as a function of whisking event duration. Pearson correlation R = 0.89, p = 0.016. N= 20 FOV in 16 mice

L) Average astrocytic Ca2+ activity in all ROIs during all volitional whisking events lasting >1s (Green) shows levels significantly above baseline both prior to and after PA dilation (red). Outline of 1 SD. T-test vs baseline: Early Ca2+ max: p= 8.7*10-153 AUC: p=0.0033, Late Ca2+ max: p= 3.4*10-171AUC p=0.00092, N=989, 20 FOV 16 mice.

M) Ca2+ activity normalized to SD values for single whisking events lasting between 1½-2½ s, aligned to whisking onset (yellow line). Above: from astrocytic ROIs, Below: from neuronal synaptic ROIs.

N) Average 2-photon image from layer II/III. Red: Texas red-dextran in vessel lumen, Green: GCaMP7 expressed in all neurons by the synapsin promotor. Blue circle outlines the synaptic ROIs within <15µm of the PA.

O) Neuronal Ca2+ averaged from synaptic ROIs within <15µm of the PA from all volitional whisking events of increasing duration.

P) The amplitude of neuronal calcium responses from synaptic ROIs within <15µm of the PA as a function of whisking event duration. Pearson correlation R = 0.94, p = 0.0053. N= 19 FOV in 7 mice.

Q) Pupil imaged by an IR camera, used to detect the arousal state of the animal in relation to volitional whisking.

R) Pupil fluctuation aligned to all volitional whisking events of increasing duration.

S) The amplitude of pupil dilation following volitional whisking of different durations. Pearson correlation R = 0.69, p = 0.12. N= 6 mice.

Enhanced deflections during volitional whisking increase early astrocytic Ca2+ responses in spatial accordance with neuronal responses.

Studies using anesthetized animals show that increased frequency of whisker stimulation triggers a more robust NVC response due to enhanced recruitment of the excitatory neurons in the barrel cortex(Jessen, Mathiesen et al. 2017). We could not control the frequency of the volitional whisking, so to increase sensory input, we enlarged the deflection of the whiskers during the volitional whisking events. We did

this by placing a piece of sandpaper within the brush of whiskers (Figure 2A). Modifying the sensory input by the sandpaper resulted in relatively larger dilations of the PA compared to whisking events of similar duration without sandpaper (Figure 2B and C) (ANCOVA, p = 0.0065, N=21 FOVs in 16 mice). The effect was insignificant on the 1st order capillary dilations (Supplemental Figure S9). This difference suggests that the increased sensory input was sufficient to increase blood flow recruiting processes in the deeper cortical layers but not strong enough to trigger an additional blood flow response in the more superficial cortical layers. The sandpaper only influenced PA dilations during extended whisking events (Figure 2C). Thus, our investigation of the cellular response to enhanced sensory input focused on volitional whisking events longer than 1.5 seconds. Even though the presence of the sandpaper did not change the whisking behavior of the mice (Supplemental Figure S10), we reduced the variation in the data by excluding volitional whisking events that lasted >3 s. After having grouped the whisking events, we confirmed the PA-specific effect measuring the expansion in absolute values of μm^2 (Figure 2D, 2E and 2I; mixed model test, PA: AUC: p=0.024, Max: p=0.0267, N= 21 FOVs in 16 mice. 1st order Capillary AUC: p=0.211, Max: p=0.129, N=10 FOVs in 7 mice). As could be expected from the lack of effect on the 1st order capillary dilations, the sandpaper did not generally affect the local neuronal responses (Figure 2F, 2I and Supplemental Figure S9D). To investigate whether cellular activity depended on nearness to the part of the vasculature and to compare between FOVs, we grouped the synaptic ROIs in 15 µm zones from the center of the PA within the FOV. We found that the neuronal response in the synaptic ROIs closest to the vessels, within 30µm of PA, was substantially increased (Figure 2F and Supplemental Figure S9D, mixed model, Max early p=0.011, Max late p=0.0275, N=20 FOV, 7 mice). Similarly, the increased sensory input also only increased astrocytic Ca2+ response in ROIs found within 30µm of the vascular inflow tract (Figure 2G, 2H, 2I and Supplemental Figure S9E and F, mixed model test, Max early=p0.00471, Max late p=0.0154 N=21 FOVs in 16 mice). Hence, early astrocytic activity was similarly affected and had the same spatial distribution as synaptic activity. This observation indicates that the first peak in the astrocytic response is due to the astrocytic proximity to the synapses, so that this astrocytic activity reflects the level of sensory-dependent neuronal excitation. Such spatial specificity is a requirement for astrocytic participation in the recruitment of the NVC response. The increased whisking deflection also significantly enlarged the second peak in the astrocytic Ca2+ response, which is proposed to correlate with or sustain the blood flow response(Institoris, Vandal et al. 2022). This increase occurred with less spatial specificity, as it was both in the astrocytes closest to the PA and in all structures independent of distance from the PA (Figure 2G and 2H and 2I, Supplemental Figure S9E and F, mixed model test Max p=0.046 N= 21 FOVs in 16 mice). The modest and localized increase in neuronal activity

achieved by sandpaper touching the whisker during volitional whisking suggests that the increased demand for blood flow is triggered by neuronal activity in deeper cortical layers. And that these recruit neurons in a position close to the relevant point of regulation in layer II/III of the barrel cortex during sensory processing. This effect was not due to any arousing or aversive effect of the sandpaper, as the pupil expansion to volitional whisking events were similar with and without sandpaper (Figure 2J, Paired T-test, p = 0.531, N=6 mice). Thus, the effect of the sandpaper on neuronal and astrocytic activity, as well as the increased PA dilation, was best explained by additional sensory excitation produced by the larger deflections of the whiskers. The spatial dependency and proportionality of astrocytic activity to neuronal responses and their position in relevant distance from the vascular inflow tract, suggests that our analysis succeeded in identifying astrocytic activity involved in recruiting NVC responses to volitional whisking. This astrocytic Ca2+ activity appears to be triggered by volitional whisking activity through increased local neuronal activity near the vessel.

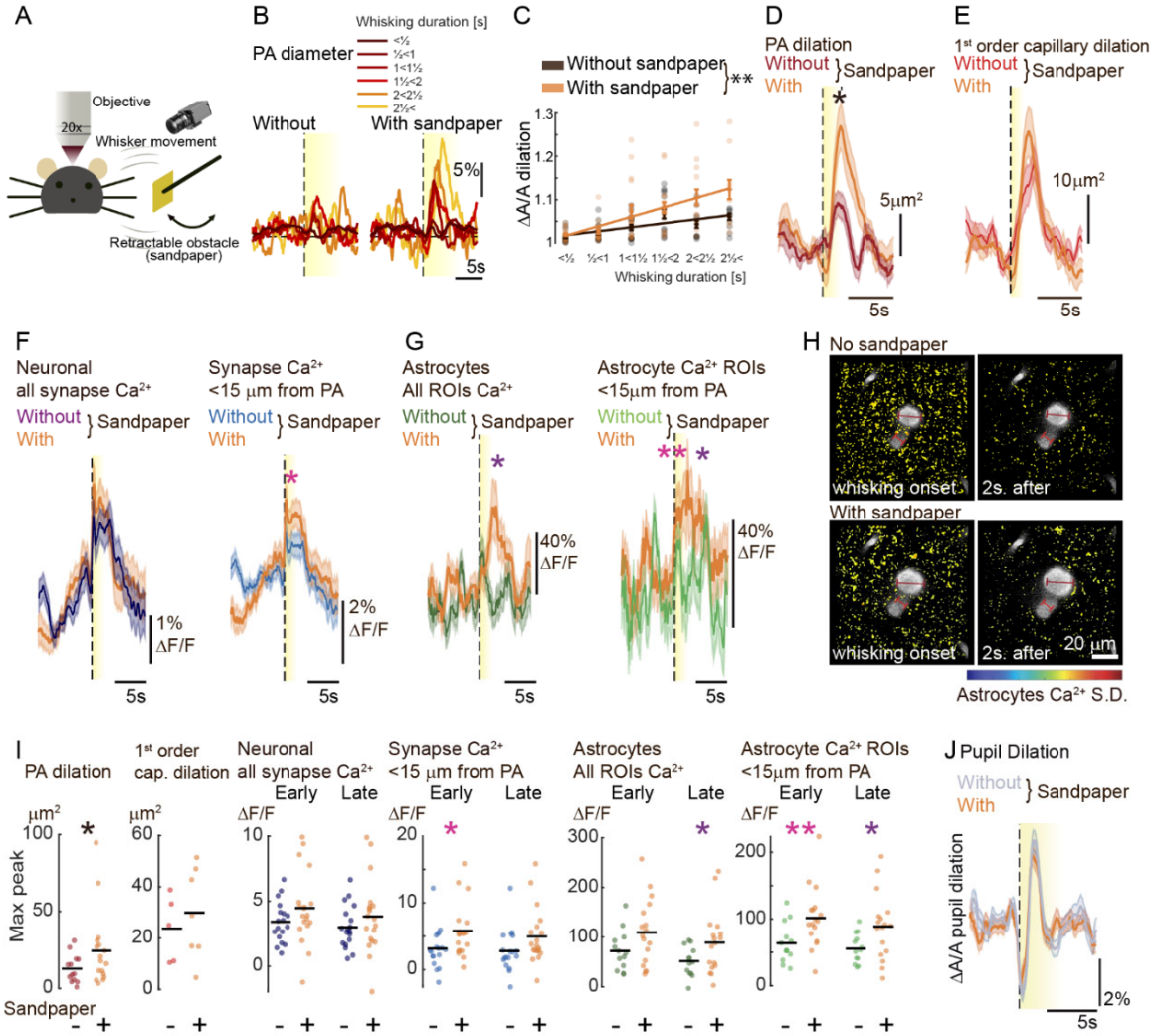

Figure text, figure 2. Increasing sensory input during volitional whisking gave stronger vasodilations and increased Ca2+ activity in the neurons and astrocytes bordering the PA.

A) Cartoon of the setup showing the principle of the retractable obstacle. An infrared camera records whisker movements and a piece of sandpaper is connected to a motorized arm to become retractable.

B) Average PA vessel dilation during volitional whisking events of increasing duration of whisking events, without (left) and with sandpaper (right).

C) PA dilation amplitude as a function of whisking duration showed significant enlargements comparing whisking with (orange) and without (black) sandpaper. N= 21 locations in 16 mice ANCOVA, **p<0.01.

D) Average PA dilation to all volitional whisking events 1½<3s long, measured in cross-area changes with (orange) and without sandpaper (dark red). Outline of 1 SD, mixed model test, PA: AUC: p=0.024, Max: p=0.0267, N= 21 FOVs in 16 mice.

E) Average 1st order capillary dilation to all volitional whisking events 1½<3s long, measured in cross-area changes with (orange) and without sandpaper (red). Outline of 1 SD, mixed model test, PA: AUC: p=0.211, Max: p=0.129, N= 10 FOVs in 7 mice.

F) Average neuronal Ca2+ levels during all volitional whisking events 1½<3s long with (orange) and without sandpaper (dark blue: All synaptic ROIs, blue: synaptic ROIs within <15µm from PA). Outline of 1 SD, Mixed model test: All: Max early p=0.088, Max late p=0.21, <15µm from PA: Max early p=0.021, Max late p=0.07, N= 19 FOVs in 7 mice.

G) Average astrocytic Ca2+ levels during all volitional whisking events 1½<3s long with (orange) and without sandpaper (dark green: All ROIs, green: ROIs within <15µm of PA). Outline of 1 SD, mixed model test, All: Max early p=0.077, Max late: p=0.049, 15µm from PA: Max early: p=0.00471, Max late p=0.0154 N=21 FOVs in 16 mice

H) Average 2-photon image from volitional whisking events without (above) and with (below) sandpaper. Ca2+ activity normalized to s.d. values per pixel over time, as shown in pseudocolor, at whisking onset, and 2. after. Overlayed greyscale image of vessels, red scalebar shows dilation of both PA (dark red) and 1st order capillary (light red).

I) Max amplitude of responses with and without sandpaper averaged pr FOV for the data shown in plots D-G.

J) Sandpaper did not affect the average pupil fluctuations during volitional whisking events 1½<3s long, with (orange) and without sandpaper (grey).

During volitional whisking, early astrocytic Ca2+ activity depends on cortical NA levels and facilitates blood flow recruitment in 1st order capillaries.

Astrocytic Ca2+ has been shown to depend strongly on NA levels(Paukert, Agarwal et al. 2014, Reitman, Tse et al. 2023). We hypothesized that astrocytic contributions to NVC could rely on the cortical levels of this neuromodulator. To investigate this, we inhibited the release of NA from locus coeruleus by treating the mice with DSP-4 48 hours before the imaging session. This neurotoxin is known to abolish the NA-releasing neuronal projections from locus coeruleus to the barrel cortex(Iannitelli, Kelberman et al. 2023) and lower the general cortical NA levels(Slezak, Kandler et al. 2019, Renden, Institoris et al. 2024). To confirm the effect on astrocytic Ca2+ activity, we detected the occurrence of long-duration surges with the dynamic ROI detection analysis (Supplemental Figure S3). We found a significant drop in regions with astrocytic Ca2+ events after the treatment (Figure 3A, T-test p=0.0043, N= 21FOVs in 16mice) as well as fewer long duration (> 5s) astrocytic Ca2+ surges in the average from ROIs not bordering the vessels (Figure 3B, T-test p=0.0039, N= 21FOVs in 16mice). We evaluated the effect on pupil dynamics to check whether DSP-4 influenced the NA release to the volitional whisking events. We found that the dilation part of the pupil activity was reduced, though not significantly (Figure 3C, Paired T-test, p=0.224, N=6 mice). This lack of significance might be explained by a general pupil-constricting effect of the neurotoxin as baseline diameter was much reduced (Figure 3D, Paired T-test, p=4.2*10-5, N=6 mice). In addition, there was a remarkable disruption in the synchronicity of the pupil dynamics as we no longer saw constriction followed by dilation with the volitional whisking onset (Figure 3E). The question was whether the volitional NVC response was intact under these circumstances. Considering the lumen of the vessels in the vascular inflow tract, the PAs dilated to the same extent as before, but the dilations of the 1st order capillary were heavily attenuated after the DSP-4 treatment (Figure 3F, mixed model, PA p=0.65, N= 21 FOVs in 16mice, 1st order cap.: p= 0.0045, N= 10 FOV in 7 mice). As NA can have a vasoconstricting effect(Montalant, Kiehn et al. 2024), we checked that the lack of capillary dilation response was not due to a baseline dilation of the vessels after depletion of the cortical NA levels. But neither the PA nor the 1st order capillary was expanded in the DSP-4 treated animals (Figure 3G, Mixed model test, PA p=0.70, N= 21 FOVs in 16 mice, 1st order cap.: p= 0.88, N= 10 FOV in 7 mice). The reduced 1st order capillary dilation response could not be explained by reduced neuronal excitation to the volitional whisking. Regardless of distance from the PA, neuronal Ca2+ responses were not reduced by the depletion of the cortical NA levels (Figure 3H, Supplemental Figure S11A and B, Mixed model, All ROIs: p=0.88, within 15µm of PA: p=0.82, N=19 FOV in 7 mice). Now, we wondered whether the reduced NA levels and the attenuation of the astrocytic Ca2+ surges had altered the astrocytic responses to

volitional whisking. Surprisingly, the effect on the astrocytic Ca2+ responses to volitional whisking was not strong. The lack of effect could not be explained by a change in whisking behavior in the DSP-4 treated animals (Supplemental figure S12). Most of the early astrocytic Ca2+ responses were intact, but there was a slight reduction in the ROIs bordering the vascular inflow tract (Figure 3I and 3J, Supplemental Figure S11C-E, mixed model test, p=0.0216, N= 21FOVs in 16mice). The relative intactness of the signal supports that the synaptic activity still triggered astrocytic Ca2+ but that the general effect of the NA depletion curbed their responsivity. The delayed Ca2+ peak following dilation was also attenuated in the ROIs bordering the vessels but not significantly in the other astrocytic ROIs (Figure 3I and 3J, Supplemental Figure S11C-E, mixed model test, within 15µm of PA: p=0.012, All ROIs: p=0.061 N= 21FOVs in 16mice). These results indicate that the early astrocytic Ca2+ activity in the cells bordering the inflow tract may play a blood flow recruiting role in the volitional NVC response of the 1st order capillaries. And that this function is dependent on adequate cortical NA levels.

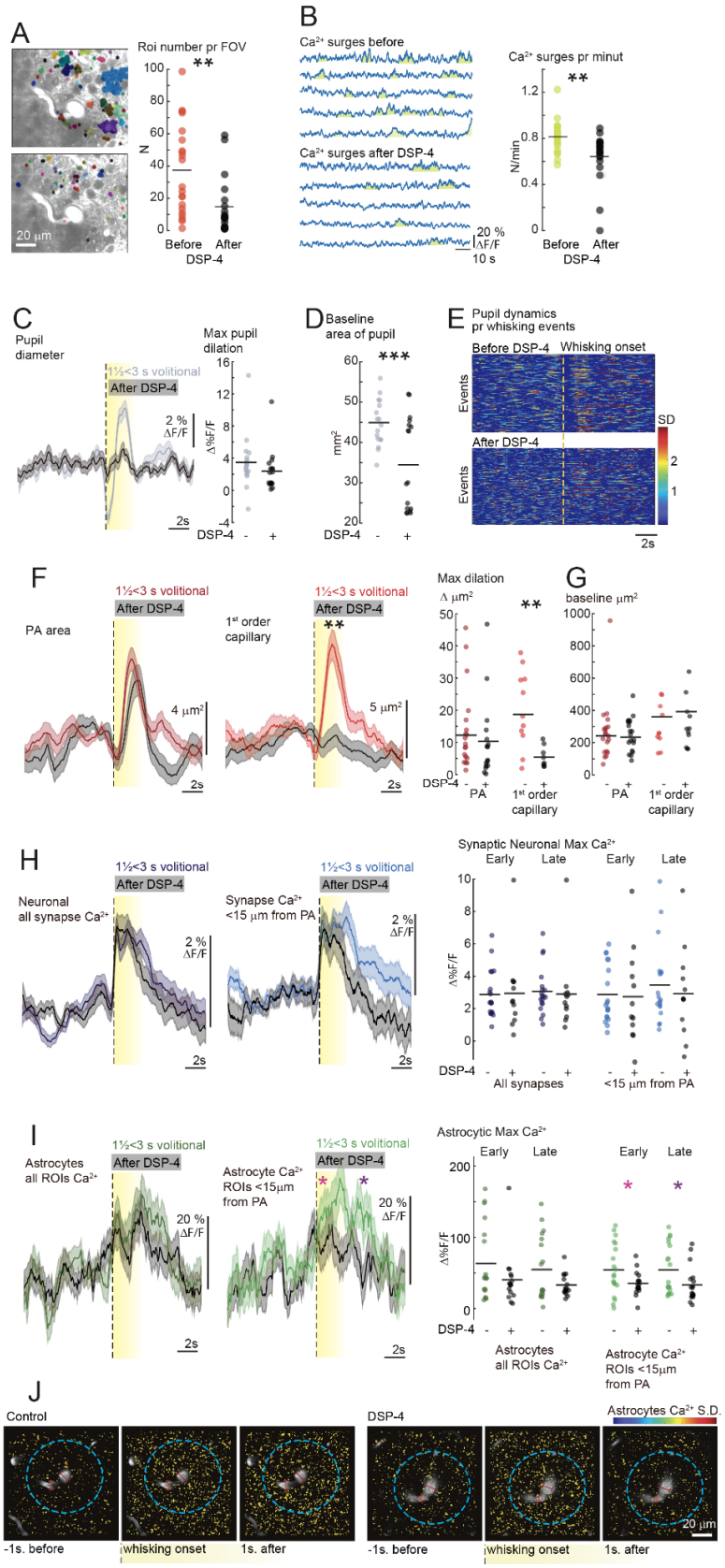
A
Roi number pr FOV
**
N
Before
After
DSP-4
20 µm
B
Ca²⁺ surges before
Ca²⁺ surges after DSP-4
20 % ΔF/F
10 s
Ca²⁺ surges pr minut
**
N/min
Before
After
DSP-4
C
Pupil diameter
1½<3 s volitional
After DSP-4
2 % ΔF/F
2s
Max pupil dilation
Δ%F/F
DSP-4
D
Baseline area of pupil
***
mm²
DSP-4
E
Pupil dynamics pr whisking events
Before DSP-4
Whisking onset
Events
After DSP-4
SD
2s
F
PA area
1½<3 s volitional
After DSP-4
4 µm²
2s
1st order capillary
**
5 µm²
Max dilation
Δ µm²
**
DSP-4
PA
1st order capillary
G
baseline µm²
PA
1st order capillary
H
Neuronal all synapse Ca²⁺
1½<3 s volitional
After DSP-4
2 % ΔF/F
2s
Synapse Ca²⁺ <15 µm from PA
Synaptic Neuronal Max Ca²⁺
Early
Late
Δ%F/F
DSP-4
All synapses
<15 µm from PA
I
Astrocytes all ROIs Ca²⁺
1½<3 s volitional
After DSP-4
20 % ΔF/F
2s
Astrocyte Ca²⁺ ROIs <15µm from PA
Astrocytic Max Ca²⁺
Early
Late
Δ%F/F
DSP-4
Astrocytes all ROIs Ca²⁺
Astrocyte Ca²⁺ ROIs <15µm from PA
J
Control
DSP-4
Astrocytes Ca²⁺ S.D.
20 µm
-1s. before
whisking onset
1s. after
-1s. before
whisking onset
1s. after

Figure text, figure 3. Depletion of noradrenergic input from the locus coeruleus and disturbance of astrocytic Ca2+ responses inhibited dilation of 1st order capillaries during volitional NVC responses in the resting mice.

A) Fewer regions of dynamic astrocytic Ca2+ surges were detected following the locus coeruleus toxic DSP-4 administration. Left: Example of ROI detection results. Right: The average number of ROIs detected pr FOV before (red) and after (black) DSP-4. T-test, p=0.0043, N=20 FOV pr 16 mice.

B) Left: Example of the reduced detection of astrocytic Ca2+ surges (duration >5s) before (above) and after (below) DSP-4. Right: Quantification of the average occurrence of astrocytic Ca2+ surges from ROIs >30µm from the PA before (green) and after DSP-4 (black). T-test, p=0.0039, N=20 FOV pr 16 mice.

C) Left: Despite DSP-4's effect on the average pupil fluctuations during volitional whisking events 1½<3s long, Right: the maximal pupil dilations were not significantly different before (grey) or after DSP-4 (black). Paired T-test, p=0.224, N=6 mice.

D) Baseline area of the pupil averaged pr mouse was constricted after DSP-4 (black). Paired T-test, p=4.2*10-5, N=6 mice.

E) Pupil dynamics normalized to standard deviation values during individual volitional whisking events lasting between 1½-3 seconds aligned to whisking onset illustrates a lack of synchronicity following DSP-4 treatment (below).

F) Average vasodilations during volitional whisking events lasting between 1½-3 seconds, Outline of 1 SD. Left: PA dilation (dark red) did not change significantly after DSP-4 (black). Middle: 1st order capillary dilation(red) was strongly reduced after DSP-4(black). Right: Quantification of the average effect on vasodilations pr FOV, show how the DSP-4 driven elimination of locus coeruleus based cortical noradrenaline release only affected 1st order capillary dilations. Mixed model, PA: p=0.65 N=20 FOVs in 16 mice, 1st order cap.: p=0.0045 N=10 FOVs in 7 mice.

G) The effect of DSP-4 treatment was not due to an impact on the average baseline cross area of neither PA (left) or 1st order capillary (right). Mixed model, PA: p=0.579 N=20 FOVs in 16 mice, 1st order cap.: p=0.578 N=10 FOVs in 7 mice.

H) Average neuronal Ca2+ in synaptic ROIs during volitional whisking events lasting between 1½-3 seconds, Outline of 1 SD. Left: All ROIs (dark blue) did not change significantly after DSP-4 (black). Middle: Responses in synaptic ROIs within <15µm of PA (blue) were also not reduced by the DSP-4 (black). Right: Quantification of the average effect of the DSP-4 treatment on neuronal Ca2+ in

ROIs pr FOV. Mixed model, All ROIs: Early p=0.88. Late p=0.82, within 15µm of PA: early p=0.82, late p=0.57, N=19 FOV in 7 mice.

I) Average astrocytic Ca2+ in ROIs during volitional whisking events lasting between 1½-3 seconds, Outline of 1 SD. Left: All ROIs (dark green) did not change significantly after DSP-4 (black). Middle: Both early and late Ca2+ peaks in ROIs within <15µm of PA (green) were significantly reduced by the DSP-4 (black). Right: Quantification of the average effect of the DSP-4 treatment on astrocytic Ca2+ in ROIs pr FOV. Mixed model, All ROIs: Early Peak p=0.12, Late peak p=0.061 within 15µm of PA: Early peak p=0.0216 Late Peak: p=0.013, N=20 FOV in 16 mice.

J) Average 2-photon image from volitional whisking events before (left) and following DSP-4 (right). Ca2+ activity normalized to s.d. values pr pixel over time shown in pseudocolor, before, at whisking onset and 1 s. after. Overlayed grey scale image of vessels, red scalebar shows dilation of both PA (dark red) and 1st order capillary (light red). Blue stippled line shows a 30µm distance from PA.

When comparing self-initiated to evoked whisking events, neuronal Ca2+ activity was earlier, while the timing of astrocytic Ca2+ and vascular responses was unchanged.

As early astrocytic Ca2+ activity has often been questioned in evoked sensory responses, we wondered if we had observed an astrocytic activity specific to self-initiated NVC responses. To test this, we compared the NVC response in volitional whisking to evoked stimulation using air puff (Figure 4A). While natural whisking is an active and expected deflection, the air puff stimulation is an unexpected sensory event. This stimulation method can startle the animal if used without caution. We minimized the air pressure to cause the smallest visible deflection to avoid arousal and ensured that the air puff only hit the whiskers. We also habituated the animal to the stimulation in training sessions before the experiment. Even so, air puff stimulation caused the animal to start running in approximately 17% of the trials, indicating some startling effect. These cases were discarded, and only stimulations that did not result in running were included. Air puff stimulation resulted in robust vasodilations of both the PA and the 1st order capillary, which were larger than the dilations during self-initiated whisking events of similar duration (Figure 4B and 4C, Welch's t-test, PA: p=0.014, Air puff N=8 FOVs in 6 mice vs. natural whisking N= 21 FOV in 16 mice, 1st order cap: p=0.0126, Air puff N=8 FOVs in 6 mice vs natural whisking N= 10 FOV in 7 mice). The increase in the NVC response with considerable expansion of both PA and 1st order capillary was matched with increased neuronal Ca2+ activity (Figure 4D, Supplemental figure S13C and D, Welch t-test,

Max early peak p = 0.013, Max late peak p=0.0194 N=19 FOV in 7 mice). The increase was in all synaptic ROIs, independent of distance from the blood vessel. Such a level of excitation justifies the substantial blood flow recruitment. The different initiations in evoked versus volitional whisking mean only the latter could involve a preemptive excitation signal to ready the sensory cortex to receive input from the anticipated whisker deflections. Indeed, the neuronal response was slightly earlier to volitional whisking than to evoked whisker deflections (Figure 4E and F, paired t-test onset (red star) p=0.0089 N=19 FOV in 7 mice). However, the function of this preemptive signal is not likely to be a blood flow recruiting one, as the onset of PA and 1st order capillary dilations were similar in the evoked versus the volitional NVC responses (Figure 4B and 4C).

The next question was how much astrocytic Ca2+ responses differed between evoked and self-initiated whisking. At first glance, astrocytic responses were delayed in evoked whisking compared to volitional (Figure 4G) as there was a delayed time to peak in evoked astrocytic calcium transients (Figure 4H, Welch's t-test, p = 0.00074, Air puff N=8 FOVs in 6 mice vs natural whisking 21 FOV in 16 mice). However, the average curve trend revealed two peaks in the astrocytic responses to the airpuff-induced NVC events. And just as we found during volitional whisking, there was one peak prior to and another after the dilation (Figure 4G). The enlarged second Ca2+ peak during evoked responses explains the difference in peak time. Comparing the amplitude of these two Ca2+ transients, the early astrocytic Ca2+ response was only slightly, though significantly larger, prior to the evoked NVC responses (Figure 4G and 4I). In contrast, the delayed activity was substantially larger to the airpuff evoked than to volitional whisking (Figure 4G and 4J, Welch's t-test, Early peak Max p = 0. 032, Late peak Max p=0.018 Air puff N= 8 FOVs in 6 mice vs. natural whisking N= 21 FOV in 16 mice). The delayed astrocytic Ca2+ response to the evoked stimulation was almost none-existent in the vessel-near astrocytic ROIs (Supplemental figure S13). Besides this slight divergence in spatial distribution, we found no difference in astrocytic Ca2+ activity between evoked and volitional NVC response, except what could be explained by enhanced neuronal excitation.

Vascular responses to evoked whisking events did not depend on cortical NA levels or reduced astrocytic Ca2+ surge activity, but neuronal responses did.

The increased early astrocytic Ca2+ peak matched the increased synaptic activity, and the much larger second peak the size of the evoked dilation. In summary, the more prominent activation of neurons, astrocytes, and vasculature in the evoked compared to volitional whisking suggests that a comparable larger deflection of the whiskers leads to a stronger sensory input and more widespread recruitment of

cortical neurons (Figure 4B-K). One possible confounding factor for this assumption was that the pupil dilated much more during air-puff evoked than volitional whisking (Figure 4L, Paired t-test, p=0.000128, N=6 mice). Thus, we suspected some arousal effect of the air-puff stimulation despite our precautions to avoid startling the animal. A small arousal response would induce an NA release in the cortex, which could influence the neuronal and astrocytic responses to the puff-evoked whisking. To investigate this, we evaluated the response to the evoked whisking in the DSP-4 treated animals. The pupil dilations were decreased, though only slightly (Figure 4L, Paired T-test, p=0.014, N=6 mice). Meanwhile, the vascular response to the airpuff evoked stimulations in both PA and 1st order capillaries was unchanged (Figure 4M and 4N, Supplemental figure S13B; t-test, PA: p=0.718, 1st order cap.: p=0.632 N=8 FOV in 6 mice). It was thus surprising that the neuronal response to the evoked stimulation was reduced. The reduction was primarily of the later peak and in synaptic ROIs more than 30µm distance from the vessel (Figure 4O; t-test, All ROIs, early peak: p=0.052, Late peak: p=0.0053 N=19 FOV in 7 mice Supplemental figure S13C and D). In accordance with the unchanged NVC response, the synaptic responses within 30µm were not affected by the absence of this NA release (Figure 4O; t-test, Paired t-test, ROIs<15µm Early peak p=0.10, Late peak p= 0.26, N=19 FOV in 7 mice Supplemental figure S13C and D). Also, the early pre-dilation astrocytic Ca2+ response remained the same (Figure 4P, Supplemental figure S13 E-G, t-test p=0.126, N=8 FOV in 6 mice). Only the late astrocytic Ca2+ response to the airpuff evoked whisker-deflection decreased slightly with the treatment (t-test p=0.018, N=8 FOV in 6 mice, Figure 4P, Supplemental figure S13 E-G). Again, the astrocytic activity was spatially dependent on neuronal synaptic excitation, as the response in the astrocytic ROIs >30µm from the vascular inflow tract was also reduced following the DSP-4 treatment (Figure 4K, Supplemental figure S13E-G). All taken together, the lack of effect of the DSP-4 treatment on the evoked NVC indicates that NA release did not contribute to this response. The differences we observed between evoked and the volitional whisking NVC could be explained by increased excitation of the barrel cortex. One remarkable difference, was that the attenuation of cortical NA levels and elimination of the astrocytic Ca2+ surges by DSP-4 did not influence the early astrocytic Ca2+ response nor the 1st order capillary dilation to the stimulation. This suggests a substantial difference in the blood flow recruiting mechanisms between evoked and volitional NVC responses.

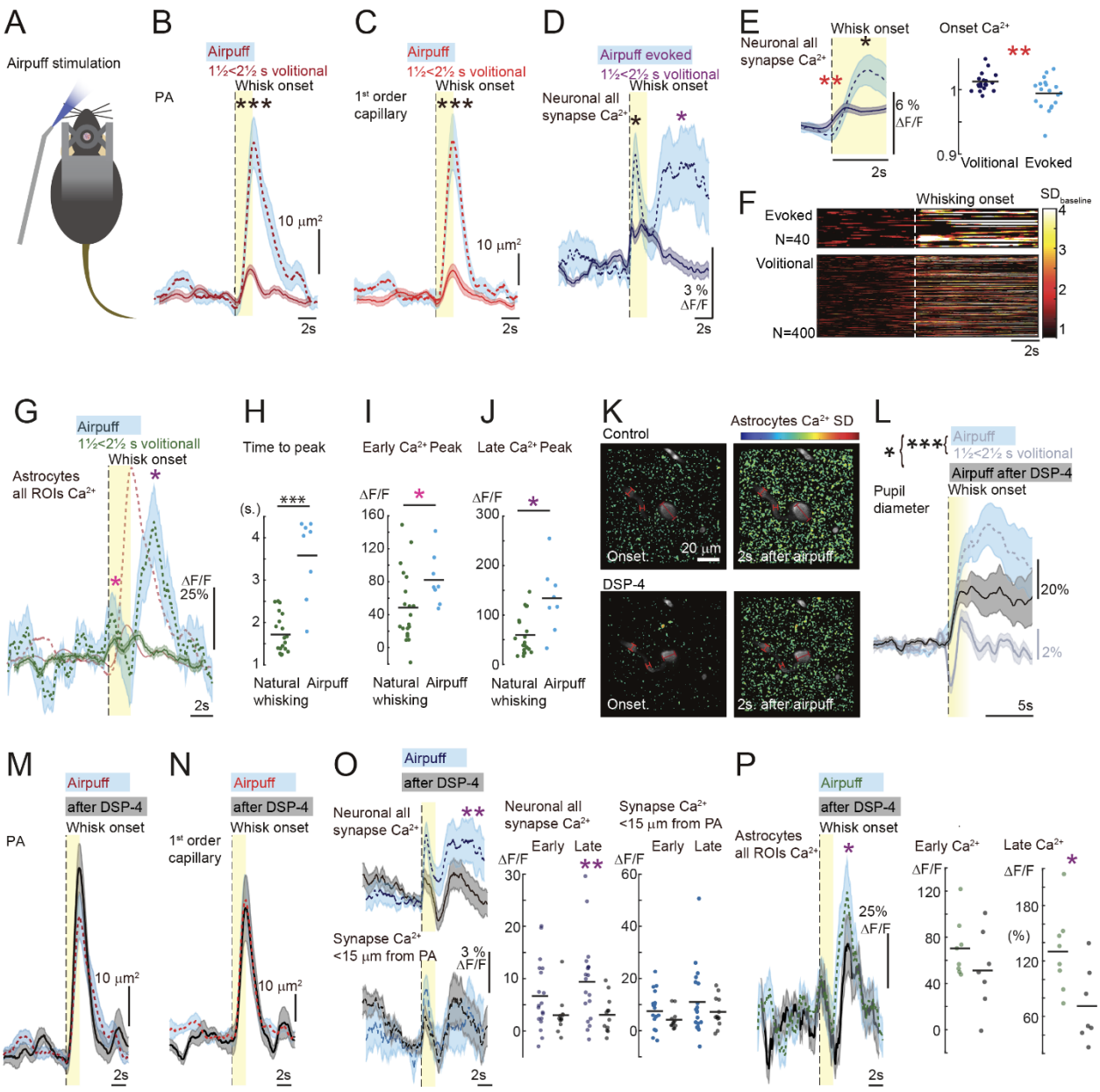

Figure text, figure 4. Evoked NVC response did not depend on cortical noradrenergic levels, but astrocytic and vasoactive responses were otherwise comparable to volitional whisking.

A) Cartoon of the evoked whisker stimulation using air puff

B) Average PA vasodilation during volitional whisking events lasting between 1½-2½ seconds (dark red, solid line) was significantly smaller than during 2s air-puff evoked whisking (stippled line, 1 SD outline in light blue). Welch's t-test, p=0.014, Air puff N=8 FOVs in 6 mice vs natural whisking N= 21 FOV in 16 mice, 1st order cap: p=0.0126, Air puff N=8 FOVs in 6 mice vs natural whisking

N= 10 FOV in 7 mice, PA: p=0.65 N=20 FOVs in 16 mice, 1st order cap.: p=0.0045 N=10 FOVs in 7 mice.

C) Average 1st order capillary vasodilation during volitional whisking events lasting between 1½-2½ seconds (red, solid line) was significantly smaller than during 2s air-puff evoked whisking (stippled line, 1 SD outline in light blue). Welch's t-test, p=0.0126, Air puff N=8 FOVs in 6 mice vs natural whisking N= 10 FOV in 7 mice.

D) Average neuronal Ca2+ during volitional whisking events lasting between 1½-2½ seconds (dark blue, solid line) were significantly smaller than during 2s air-puff evoked whisking (stippled line, 1 SD outline in light blue). Paired t-test, Max early peak (black) p = 0.013, Max late peak (dark blue) p=0.0194, N=19 FOV in 7 mice,

E) Left, Average neuronal Ca2+ from synaptic ROIs zoom in from C). Right: Quantified onset Ca2+ levels (0-100ms after whisking onset) averaged pr FOV. Neuronal Ca2+ in all synaptic ROIs rose significantly earlier to volitional whisking (dark blue, solid line) than to evoked whisking (stippled line, 1 SD outline in light blue). Paired t-test, Onset level (red stars) p=0.0089 N=19 FOV in 7 mice, black star same as in D).

F) Neuronal Ca2+ activity average from all synaptic ROIs normalized to SD values shown in pseudocolor scale. For single whisking events, aligned to whisking onset (yellow line). Above: Air-puff evoked, Below: from volitional whisking events lasting between 1½-2½ s.

G) Average astrocytic Ca2+ during volitional whisking events lasting between 1½-2½ seconds (dark green, solid line) were significantly smaller than during 2s air-puff evoked whisking (stippled line, 1 SD outline in light blue). Average PA dilations from B) reveal how both responses rose in two peaks, one before and one after the vasodilations.

H) Comparing time to Max peak of the astrocytic Ca2+ response in F) shows that the second Ca2+ peak is the largest in the evoked response (blue). Welch's t-test, p = 0.00074, Air puff N=8 FOVs in 6 mice vs natural whisking 21 FOV in 16 mice.

I) The amplitude of the early peak (pink star) in the Ca2+ response from F) shows that evoked responses were larger than the volitional. Welch's t-test, Early peak Max p = 0. 032 puff N= 8 FOVs in 6 mice vs. natural whisking N= 21 FOV in 16 mice.

J) The amplitude of the late peak (purple star) in the Ca2+ response from F) was even larger in the evoked responses than the volitional. Welch's t-test, Late peak Max p=0.018 Air puff N= 8 FOVs in 6 mice vs natural whisking N= 21 FOV in 16 mice.

K) Average 2-photon image from air puff evoked events before (above) and following DSP-4 (below). Ca2+ activity normalized to s.d. values pr pixel over time shown in pseudocolor, 2 and 4 seconds after air puff. Overlayed grey scale image of vessels, red scalebar shows dilation of both PA (dark red) and 1st order capillary (light red).

L) Average pupil dilations during volitional whisking events lasting between 1½-2½ seconds (grey, solid line) were significantly smaller than during 2s air-puff evoked whisking (stippled line, black, 1 SD outline in light blue). Paired t-test, p=0.000128, N=6 mice. DSP-4 (black, solid line, SD outline in dark grey) reduced the response, paired t-test p=0.014, 6 mice.

M) Average PA vasodilations during 2s air-puff evoked whisking (Dark red stippled line, 1 SD outline in light blue) were not significantly changed by DSP-4 black (solid line, black, SD outline in dark grey). Paired t-test, p=0.718, N=8 FOV in 6 mice.

N) Average 1st order capillary vasodilations during 2s air-puff evoked whisking (Red stippled line, 1 SD outline in light blue) were not significantly changed by DSP-4 black (solid line, black, SD outline in dark grey). Paired t-test, p=0.632 N=8 FOV in 6 mice.

O) Average neuronal Ca2+ in synaptic ROIs during 2s air-puff evoked whisking. (All ROIS, Dark blue stippled line, 1 SD outline in light blue), was significantly reduced by DSP-4 black (solid line, black, SD outline in dark grey). Paired t-test, All ROIs Early peak p=0.052, Late peak p= 0.0053, ROIs<15µm Early peak p=0.10, Late peak p= 0.26, N=19 FOV in 7 mice.

P) Average astrocytic Ca2+ in all ROIs during 2s air-puff evoked whisking (Dark green stippled line, 1 SD outline in light blue) was only significantly changed by DSP-4 (solid line, black, SD outline in dark grey) in the late peak of the response. Paired t-test, Early peak p=0.24, Late peak p=0.018, N=8 FOV in 6 mice.

During locomotion, the whisking-based NVC response no longer correlated with the response size in neither neurons nor astrocytes.

So far, we have only considered NVC response to whisking deflections in the resting animals. However, an essential part of locomotion is that animals continuously whisk while moving (Supplemental Figure S2). In addition, any locomotion would be preceded by volitional whisking for 0.5±0.13 before the onset of locomotion. This initial whisking is a reasonable behavior of surveillance prior to the increase in movement speed, as mice primarily rely on their whiskers to explore the surroundings. Evidently, the excessive whisking during locomotion provides a strong excitation of the sensory pathway. Locomotion is also associated with arousal, which entails the release of NA to many parts of the sensory cortices,

including the barrel cortex(Shimaoka, Harris et al. 2018). As astrocytes are known to respond to NA in arousals, we hypothesized that the widespread NA release from locus coeruleus modified astrocytic contribution to volitional NVC. Like others before(Ding, O'Donnell et al. 2013, Tran, Peringod et al. 2018, Oe, Wang et al. 2020, Renden, Institoris et al. 2024), we found that locomotion evoked strong vasodilations and large, synchronous, and widespread astrocytic Ca^{2+} responses across the entire field of view (FOV) (Figure 5A, 5B and 5C). The locomotion-related astrocytic Ca2+ peaked later than the dilation of both the PA and the 1st order capillary (Supplemental Fig S14B, Wilcoxon test, PA p = 3.33e-16, 1st order capillary p = 3.8e-11 N=177 locomotion events in 16 mice). More relevant for the blood flow recruitment, the onset of the astrocytic Ca2+ response was prior to the vasodilation onset (Figure 5D, Rank sum, p = 0.047, N=177 locomotion events in 16 mice). And both astrocytic and vascular responses began after whisking onset and prior to locomotion (Figure 5D, Rank sum, ast. Ca^{2+} p = 5.9*10-5, PA p = 0.0029, N=177 Events in 16 mice). Hence, locomotion-related changes in blood flow and cellular activity in the barrel cortex occur well before the animal begins to move. This implies that the response in the barrel cortex is primarily due to the increased sensory input as a consequence of the whisking. The sensory input from the whiskers may not act alone during locomotion, as we found a remarkable pupil expansion compared to whisking events of similar duration in the resting animals (Figure 5E, paired t-test, p=5,9*10-6, N=6 mice). This expansion reveals a brain state switch and a cortical release of NA. To investigate the contribution of this locomotion-related brain state switch to the whisking-based NVC response, we compared it with responses to whisking events of similar duration in the resting animal. As expected, both PA and 1st order capillary dilations were substantially increased by locomotion (Figure 5F, mixed model test, PA: p=4,1*10-10, N= 20 FOV in 16 mice, 1st order cap: p=9,3*10-5 N= 10 FOV in 7 mice). Synaptic activation did not explain this increase well, as neuronal Ca2+ was not concurrently increased. During locomotion, a second Ca2+ peak was formed with levels significantly above what was seen in the resting animal (Figure 5G, mixed model, Early peak: p=0.67, Late peak: p=0.0061 N=19 FOV in 7 mice, supplemental Fig S14C and D). This second peak likely reflects the prolonged whisking during the locomotion. Still, it cannot be the recruiting factor in the enlarged vascular response as it only rises as vessels begin to constrict (supplemental Figure S14C). Considering the astrocytic Ca2+ responses, these also increased during locomotion, and this increase was also only significant in the post-dilation part of the response (Figure 5H, mixed model test, Early Ca: p=0.26, Late Ca: p=0.0016, N=20, FOV, 16 mice, supplemental Fig S14E). As in the neuronal synaptic activity, the second and more prominent peak in astrocytic Ca2+ seems to rise as the PA begins to constrict back to pre-whisking size (Figure 5C). Thus,

vasodilation was not as well explained by pre-dilatory neuronal and astrocytic activity during locomotion as in volitional and evoked whisking during rest.

Depletion of locus coeruleus-dependent NA release did not affect neurovascular coupling during locomotion, but the curbing effect on NVC initiation lengthened the transit time from resting whisking to locomotion.

To investigate the astrocytic contribution to the whisking-based NVC responses during locomotion, we returned to the DSP-4 treated animals. In these, we found that the vasodilatory response to locomotion was not affected (Figure 5I and 5J, Mixed model, PA: p=0.39, control N=20 FOV 16 mice and DSP-4 N=19 FOV in 14 mice, 1st order cap: p=0.49, control N= 10 FOV and DSP-4 N=11 FOV in 7 mice). Similarly, there was no significant change to neuronal Ca2+ responses following the DSP-4 treatment (Figure 5K, mixed model test, Early peak: p=0.68, late peak p=0.12, N=19 FOV in 7 mice), particularly not in the synaptic regions closest to the vessel (<15µm distance, Supplemental Figure S14F). Running-evoked astrocytic Ca^{2+} activity has previously been shown to be due to noradrenaline release from the locus coeruleus(Slezak, Kandler et al. 2019). Therefore, we expected the astrocytic Ca2+ responses to decrease in the NA-depleted animals. Indeed, after the administration of DSP-4, the bigger second peak of the astrocytic Ca^{2+} response was almost completely abolished (Figure 5L). However, looking closer at the remaining astrocytic Ca2+ dynamics after the DSP-4 treatment, the early response was intact (Figure 5L, right). This early activity was easy to overlook prior to the DSP-4 treatment, as the dimensions of the NA-based second Ca2+ peak ramp-up upon the locomotion initiation. We quantified the early astrocytic Ca2+ response and found that it was not reduced after the DSP-4 treatment (Figure 5M, Supplemental Figure S14G, mixed model test, Early Ca: p=0.22, Late Ca: p=0.017, control N=20 FOV in 16 mice, DSP-4 N=19 FOV in 14 mice). This indicates that the early peak in astrocytic Ca2+ still correlates with neuronal activity during locomotion and does not disappear with reduced cortical levels of NA. In our locomotion investigation, we aligned the cellular and vascular activity to the whisking onset rather than the locomotion onset since the investigation of NVC regulation was done in the whisker barrel cortex to which the main excitatory input is expected to be from whisker deflections. Interestingly, the only behavior change we could detect following DSP-4 treatment was with regards to this interval between whisking onset and locomotion onset (Figure 5N, Supplemental Figure S12). Following depletion of the locus coeruleus projections, the mouse whisked for 1±0.13s before locomotion onset. In contrast, the untreated animal would only whisk 0.55±0.14s before transitioning to the subsequent behavior (Figure 5N, Wilcoxon test p=0.038, Control: N= 16 mice and DSP-4 N= 13 mice). We wondered whether this

could be due to an effect of DSP-4 on the NVC in the whisking period prior to locomotion, similar to what we found in the resting animals. As we saw an impaired blood flow recruitment to the 1st order capillary during volitional whisking in the resting animal (Figure 3), we evaluated whether a similar blockade was present before locomotion onset. The difficulty in observing this was that we could only focus on locomotion events preceded by a substantial period of volitional whisking, not to confound our results by mechanisms recruiting blood flow during locomotion. Thus, our last investigation only included locomotion events with >1.5s of lag between whisking and locomotion onset. Despite the reduction in the amount of data, we could indeed detect that the initial dilation of the 1st order capillary dilation was significantly reduced (Figure 5O-P, Mixed model test, p=0.042 control: N=8 FOV, in 7 mice, after DSP-4 N=8 FOV in 6 mice). This indicates that the local blood flow regulation is impaired, at least until the transition to locomotion has occurred. We thus also expected a similar effect of the DSP-4 treatment on astrocytic Ca2+ responses in the period of whisking leading up to locomotion. To investigate whether there was a reduction of the earliest peak in the astrocytic ROIs close to the vessel, we compared the maximal Ca2+ level in the first second after whisking onset leading up to locomotion, comparing before and after DSP-4 (Figure 5Q-R, Mixed model test, p=0.36 control: N=8 FOV, in 7 mice, after DSP-4 N=8 FOV in 6 mice). Unfortunately, since the astrocytic Ca2+ data suffer from a higher degree of uncertainty than the vascular dilation, we could not conclude that the reduction in the early astrocytic response prior to locomotion was significant. Still, we already know that the neurotoxin modifies the spontaneous astrocytic Ca2+ activity (Figure 3 A-B), which may be equally critical for recruiting the 1st order capillaries in the NVC response. The slight disturbance in behavior elicited by the DSP-4 treatment could suggest an important role of the NA-dependent astrocytic Ca2+ levels and sufficient 1st order capillary blood flow in whisking barrel cortex processing of sensory input.

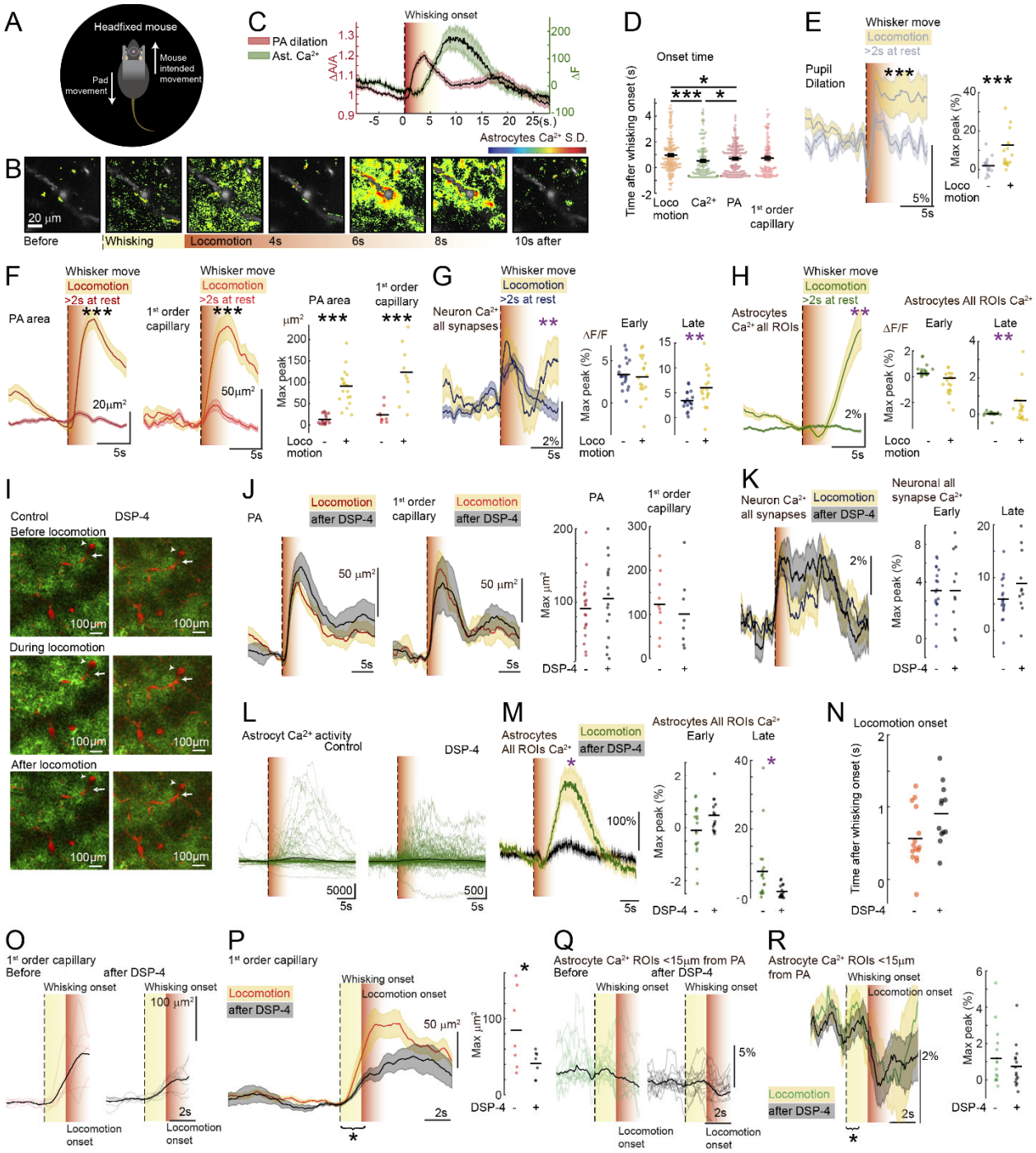

Figure text, figure 5. Depletion of locus coeruleus-dependent NA release did not affect neuron-astrocyte-vascular coupling during locomotion. Still, the curbing effect on NVC initiation lengthened the transit time from resting whisking to locomotion.

A) Cartoon of Neurotar system recording speed and direction of movement.

B) The image series averaged 1s intervals before and during locomotion. Grey: Vessel lumen, Pseudocolor: Astrocytic Ca2+ levels in s.d. normalized per pixel over time.

C) Averages of all locomotion events aligned to the whisking onset. The orange area marks the period after whisking onset wherein locomotion began. PA vasodilation and Ca^{2+} activity in all astrocytic ROIs N=177 locomotion events in 16 mice.

D) Onset time of activity from whisking onset associated with locomotion. The Ca^{2+} response (Wilcoxon test, p = 5.9*10-5) and the vasodilation (Wilcoxon test, p = 0.029) started before the locomotion while all responses lagged behind the whisking onset. The onset of astrocytic Ca2+ responses was significantly earlier than the vasodilation (Wilcoxon test, p = 0.047). N=177 locomotion events in 16 mice.

E) Left: Average pupil fluctuations during volitional whisking events >2s long (grey, solid line) were significantly smaller than during >2s locomotion (1 SD outline in yellow). Right: Quantification of max amplitudes averaged pr mouse, Paired t-test p = 5.9*10-6, N=6 mice.

F) Vasodilations were significantly larger during >2s long whisking events in locomotion than in rest. Left: Average PA dilations (SD outline dark red) during rest (dark red outline) and locomotion (SD outline yellow). Middle: 1st order capillary dilation (red) during rest (SD outline red) and locomotion (SD outline in yellow). Right: Quantification of max amplitudes averaged pr. FOV, Mixed model: PA p = 4.1-10-10 N=20 FOVs in 16 mice, 1st order cap.: p=9.4*10-5 N=10 FOVs in 7 mice.

G) Left: Average neuronal Ca2+ from synaptic ROIs (dark blue) were significantly larger in >2s long whisking events during locomotion (SD outline yellow) than in rest (SD outline dark blue). Right: Quantification of max amplitudes averaged pr FOV, Mixed model test: Early peak: p=0.68, Late peak p = 0.0060 N=19 FOVs in 8 mice.

H) Left: Average astrocytic Ca2+ from all ROIs (dark green) were significantly larger in >2s long whisking events during locomotion (SD outline yellow) than in rest (SD outline dark green). Right: Quantification of max amplitudes averaged pr FOV, Mixed model: Early peak: p = 0.28, Late peak: p=0.0016, N=20 FOVs in 16 mice.

I) Example fluorescence images before (top), during (middle), and after (below) locomotion before (left) and after (right) administration of DSP-4. Arrows without stalk point to a penetrating arteriole and with stalk point to a 1st order capillary.

J) DSP-4 increased average vasodilations during >2s locomotion events. Left: Average PA dilations before (dark red, yellow SD outline) and after DSP-4 (black, grey SD outline). Middle: 1st order

capillary dilation (red, yellow SD outline) and after DSP-4 (black, grey SD outline). Right: Quantification of max amplitudes pr locomotion event. Mixed model: PA p = 2.8*10-5 control N=93 events in 16 mice, DSP-4 N=112 locomotion events in 13 mice, 1st order cap.: p=0.075 control N=42, DSP-4 N=68 locomotion events in 7 mice.

K) Left: Average neuronal Ca2+ in all synaptic ROIS during locomotion (dark blue, yellow SD outline) was slightly increased after DSP-4 (black, grey SD outline). Right: Quantification of max amplitudes pr locomotion event. Mixed model: Early peak: p = 0.68, Late peak: p=0.12 control N=86 and DSP-4 N=48 Events in 8 mice.

L) Astrocytic Ca2+ average over all ROIS during all locomotion events before (left) and after DSP-4 (right).

M) Left: Average astrocytic Ca2+ in all ROIS during locomotion before (dark green, yellow SD outline) and after DSP-4 (black, grey SD outline). The late peak in astrocytic Ca2+ was reduced after DSP-4. Right: Quantification of max amplitudes pr locomotion event. Mixed model, Early peak: p = 0.019, Late peak p=0.00053, control N=93 events in 16 mice and DSP-4 N=112 locomotion events in 13 mice.

N) Delay from whisking onset to locomotion onset in all locomotion events was shorter before than after DSP-4 treatment. Wilcoxon test p=3.94*10-5, Control: N=177 events in 16 mice and DSP-4 N=142 locomotion events in 13 mice.

O) Dilation responses in 1st order capillaries in >1.5 s whisking (yellow) leading up to locomotion (red) averaged pr FOV before (left, red traces) and after DSP-4 treatment (right, black traces).

P) Left: Mean of the 1st order capillary dilations in O), with 1 S.D. outline. Right: Mean max peak pr FOV. Wilcoxon test, p=0.042, control: N=8 FOV in 7 mice, after DSP-4 N=8 FOV in 6 mice.

Q) Astrocytic Ca2+ response from ROIs <15µm from PA in >1.5 s whisking (yellow) leading up to locomotion (red) averaged pr FOV before (left, green traces) and after DSP-4 treatment (right, black traces).

R) Left: Mean of Astrocytic Ca2+ response in Q), with 1 S.D. outline. Right: Mean max peak pr FOV. Wilcoxon test, p=0.36 Astrocytic Ca2+ response from ROIs <15µm from PA, control: N=8 FOV, in 7 mice, after DSP-4 N=8 FOV in 6 mice.

Discussion

This study is the first investigation of astrocytic contribution to NVC in volitional whisking in the resting animal. To quantify this, we had to develop a code that could identify the astrocyte regions with spatial and temporal recurrent activity in relation to the NVC event. We found astrocytic activation within these regions during all NVC events, regardless of whether the increased sensory input was volitional or evoked, during rest or locomotion. Hence, we show that astrocytes may partake in blood flow recruitment during any NVC response in the whisker barrel cortex and during any brain state transition associated with the increased whisking. Using a neurotoxin to demolish NA release from locus coeruleus projecting neurons, we could identify that the NA-dependent astrocyte activity was necessary for the local additional blood flow recruitment in volitional whisking events during rest. The NVC response to evoked whisking or during locomotion was not reduced, likely due to a different NA dependence in the mechanisms involved during these brain state transitions. Neither was the early astrocytic peak, so our data does not exclude an astrocytic contribution to NVC to evoked whisking during locomotion. Finally, we found that the DSP-4 treated animals had a change of behavior that could suggest a critical role in the astrocyte-mediated regulation of NVC in the whisker barrel cortex as the mouse transitions from the pre-locomotion whisking to the initiation of locomotion.

Astrocyte intracellular Ca2+ activities depend greatly on anesthesia and changes with brain states(Thrane, Thrane et al. 2012, Paukert, Agarwal et al. 2014, Reitman, Tse et al. 2023). Thus, we investigated how astrocytic activity was involved in NVC responses in the whisker barrel cortex in awake and unregulated mice. We studied the vascular and cellular responses generated when the mouse voluntarily moved its whiskers and compared them to an evoked whisker stimulation. With a volitional sensory information intake, the sensory input's subsequent processing might be anticipated by the barrel cortex, and both its initiation and handling depend on arousal state (Poulet and Crochet 2018). We focused our investigation on the vascular inflow tract(Grubb, Cai et al. 2020, Hartmann, Coelho-Santos et al. 2022). Here, the penetrating arteriole (PA) dives into the cortex to sustain blood flow delivery to an extended region of the cortex. Down along its length, 1st order capillaries branch off, ensuring local and partly layer-dependent additions in blood flow. We found that the duration of the whisking activity was a strong indicator of the size of the NVC response in the form of a PA and 1st order capillary dilation. The correlation with whisking duration in the dilations of both these vascular compartments, as well as the activity of the surrounding neuron, revealed an obvious NVC response, even in the shortest whisking events. Astrocyte Ca2+ activity was seen to fall in two peaks. One preceding and one following the dilations. We found that the first astrocytic Ca2+ peak, independent of whether the whisking was evoked, volitional during rest, or volitional prior to locomotion, reflected the neuronal excitation as an

indicator of the astrocytic ability to sense neuronal synaptic transmission. We found this activity in small ROIs, whose position was identified with a context-dependent method. This method relies on timing and recurrence rather than response size. The Ca2+ activity measured within these ROIs was not randomly distributed but followed a pattern of spatial reproducibility that supports that these regions are indeed biologically relevant entities. These results supported its relevance despite the bias introduced by how the regions were selected. Because the astrocytic activity within these ROIs correlated with the neuronal activity both with regards to distance from the vessel and response size during different kinds of whisking, we propose they are the result of activation of perisynaptic processes reacting to neurotransmitter release(Santello, Toni et al. 2019, Arizono, Inavalli et al. 2020). A relationship between synaptic activity and astrocytic Ca2+ response has been proposed by numerous studies(Bindocci, Savtchouk et al. 2017, Lind, Jessen et al. 2018, Stobart, Ferrari et al. 2018, Arizono, Inavalli et al. 2020, Armbruster, Naskar et al. 2022), but never before shown in the context of awake, volitionally whisking animals. We did these observations in the unperturbed mouse and after the pharmacological elimination of the locus coeruleus-dependent noradrenaline release(Iannitelli, Kelberman et al. 2023). In the latter, we found that when sensory input was anticipated, blood flow responses depended on astrocytic Ca2+ levels in the resting animals. Depletion of the noradrenaline levels led to attenuation of the earliest part of the astrocytic Ca2+ activity in the area closest to the vessels. Meanwhile, neuronal activity and PA dilation were not disturbed. Still, the volitional triggered NVC regulation was significantly impaired, as there was no longer a dilation of the 1st order capillaries constituting the first point of entrance from the vascular inflow tract and into the tissue within the FOV. This observation is in line with previous works showing astrocytic regulation of contractile capillaries(Mishra, O'Farrell et al. 2014, Biesecker, Srienc et al. 2016, Krogsgaard, Sperling et al. 2023). The spatial arrangement of NVC-relevant neuronal and astrocytic activity in the vascular inflow tract's proximity (<30 µm) has not been described before. We identify that it is the smaller neuronal structures (<1µm^2) closest to the penetrating arteriole (PA) that show the best correlation to the length of the whisking activity. We also found a pre-emptive neuronal Ca2+ activity, which occurred in volitional but not evoked whisking. This response did not appear to influence the timing of the NVC response. Still, it is possible that it is the basis of the early astrocytic activity that facilitates capillary dilation in the volitional whisking response. One may speculate that the spatial distribution of the cellular activity could reflect that our study is done in layer II/III, which is secondarily excited as the first direct input from the thalamus is to cortical layer IV. This means that the triggering cellular and vascular responses may not primarily occur in the same layer as the one targeted by our FOV. Another unknown is the nature of the neuronal activity during the different whisking events.

Under the synapsin promoter, the Ca2+ indicator is also expressed in all neurons, and it is impossible to distinguish between Ca2+ responses from excitatory and inhibitory neurons. Such distinction could be relevant when measuring the degree of excitation because these different groups of neurons also contribute to the NVC regulation(Howarth, Mishra et al. 2021).

Until now, most studies of NVC in the whisker barrel cortex have used a forced stimulation protocol. In anesthetized mice, this may be electrical(Wang, Lou et al. 2006, Lind, Brazhe et al. 2013, Mishra, Reynolds et al. 2016) or in awake stimulations like air puff or mechanical whisker deflection (Ding, O'Donnell et al. 2013, Stobart, Ferrari et al. 2018, Tran, Peringod et al. 2018, Sharma, Gordon et al. 2020, Renden, Institoris et al. 2024). However, this approach can be problematic due to the lack of cognitive involvement of the mouse. Several intracerebral signaling mechanisms alert the sensory cortex to an impending sensory input and may participate in NVC, but their contribution can obviously not be studied using evoked stimulation. The intracerebral signaling mechanisms include synaptic input directly from the whisker motor cortex(Kinnischtzke, Simons et al. 2014) and neuromodulators released by projections from the locus coeruleus and the brain stem (Kim, Jung et al. 2016, Collins, Francis et al. 2023). The mechanisms involved may depend on whether the whisking is just regular surveillance or there is a change in the alertness of the animal(Shimaoka, Harris et al. 2018). To target this problem, we focused on volitional whisking. Until now, only a few studies have looked at the vascular responses evoked by volitional whisking of the mice(Winder, Echagarruga et al. 2017, Tran, Peringod et al. 2018, Bojarskaite, Bjornstad et al. 2020) and all but one focused on transitions between periods with more or less whisking. These transitions reflect changes in the general behavioral states, such as from sleep to awake or from a quiet wake state to a state of increased general whisking activity. Running is strongly associated with whisking(Sofroniew, Cohen et al. 2014, Collins, Francis et al. 2023) and evokes both a strong NVC response and astrocytic calcium responses(Ding, O'Donnell et al. 2013, Wang, Jang et al. 2016). Sensory evoked responses have classically been understood in the context of enhanced local synaptic activity(Devor, Ulbert et al. 2005). However, a recent study revealed activity in adrenergic projections from the locus coeruleus that correlated well with even the shortest whiskings (Collins, Francis et al. 2023). This study described less correlation with the locomotion events, which makes it even more relevant to distinguish between whisking without or during locomotion. One previous study showed a correlation between neuronal activity and CBF changes in the cortex of unstimulated, naturally whisking resting mice(Winder, Echagarruga et al. 2017). Our study expands on this observation by distinguishing between whisking of different duration as a measurement of the amount of sensory input. We also compared the response to evoked NVC response. In previous studies of evoked NVC the whiskers were

rhythmically deflected by the experimenter and often much longer stimulations were applied (Lind, Brazhe et al. 2013, Institoris, Vandal et al. 2022). Our results indicate that whisking stimulation longer than 10 s does not reproduce a natural whisking activity in the resting animal. Our results are the first to show that the earliest astrocytic Ca2+ activity can play a blood flow recruiting role in volitional NVC responses. This observation suggests more dependence on astrocytic Ca2+ activities in volitional excitation over evoked, which could be meaningful in the context of the emerging understanding of the astrocyte as a regulator of changes in brain states and thus in shifts in attention (Oe, Wang et al. 2020, Reitman, Tse et al. 2023). The reduced levels of NA following the DSP-4 treatment might thus impair the perception of the sensation from the whisking, which could contribute to a loss of focus of the mouse to the sensory input(Cerpa, Piccin et al. 2023). An indication that this might be the case was a longer delay from whisking onset to locomotion onset in the DSP-4 treated animals (Figure 5N). Considering the diminished blood flow recruitment in the 1st order capillary during volitional whisking during rest and prior to locomotion (Figure 2, Figure 5O), an effect of insufficient or delayed blood flow supply might also hinder the perception of the sensory input from the mouse while the lack of NA release suppress the decision to begin locomotion(Devilbiss 2019). To summarize, we found a remarkably different sensitivity to NA depletion between the NVC responses to the three different kinds of whisker deflections. Both astrocytic, neuronal and vascular compartments reacted differently, between volitional whisking, evoked whisking and during locomotion. This finding may have implications for understanding how patients respond to sensory input in different brain state and emotional contexts.

Materials and Methods

Animals

All procedures were performed in compliance with the guidelines from the European Council's Convention for the Protection of Vertebrate Animals Used for Experimental and Other Scientific Purposes and approved by the Danish National Ethics Committee. All experiments were performed on either WT C57bl/6j-, VGAT-ChR2-EYFP-, PV-ChR2-EYFP- or GLAST-GCaMP6-mice all of a C57bl/6j-background. GLAST-GCaMP6 mice were injected IP with 100mg/kg tamoxifen in corn oil five days in a row to induce expression of the transgene. Except for the GLAST-GCaMP6 mice, all animals were injected with either 3x200nL AAV5-gfaABC1D-lck-GCaMP6f or AAV9-syn-jGCaMP7f. Both male and female animals were used. Animals were group-housed both prior to and after chronic window implantation. Animals had access to food and water *ad libitum* and were kept on a 12/12 hour night/day cycle. Animals

were at least 8 weeks old at the time of chronic window implantation, and all experiments were performed between the ages of 10 and 38 weeks.

Chronic window implantation and viral vector injection

Chronic window implantation procedures were as in(Bindocci, Savtchouk et al. 2017). Both chronic window implantation and viral vector injection procedures were performed under aseptic conditions and isoflurane anesthesia (5% induction, 1.5% during surgery in 10% O_2 in air mixture). Before surgery, animals were injected with dexamethasone (4.8 mg/g BW; Dexavit, Vital Pharma Nordic). The fur on top of the animal's head was shaved off, and animals were placed in a stereotaxic frame on a heating pad to maintain 37°C body temperature. Eyes were kept moist using eye ointment (Viscotears, Novartis). The shaved skin was disinfected with chlorhexidine/alcohol (0.5%/74%; Kruuse). Carprofen (5 mg/kg BW; Norodyl, Norbrook) and buprenorphine (0.05 mg/kg BW; 19 Temgesic, Indivior) were administered subcutaneously as was a dose of 0.5mL saline distributed over several sites to keep the mouse hydrated during surgery. Lidocaine (100 µL 0.5%) was subcutaneously injected under the scalp. The scalp was removed, and the surface of the skull was cleaned. A small burr hole was drilled within the intended site for the craniotomy, and three doses (200nL) of AAV were deposited using a glass micropipette. Subsequently, a craniotomy was performed over the right somatosensory cortex (3 mm lateral, 0.5 mm posterior to bregma; Ø=3 mm). The bone flap was carefully removed, and the exposed brain was temporarily covered with a hemostatic absorbable gelatin sponge (Spongostan®, Ferrosan, Denmark) pre-wetted with ice-chilled aCSF. The cranial opening was filled with aCSF, then sealed with an autoclave sterilized round imaging coverslip (Ø=4 mm, #1.5 thickness; Laser Micromachining LTD). The rim of the coverslip was secured with a thin layer of GLUture topical tissue adhesive (Zoetis), and a lightweight stainless steel head plate (Neurotar) was positioned on the top of the skull surrounding the cranial window. The skull was coated with adhesive resin cement (RelyX Ultimate, 3M) to secure the exposed bone, including the skin incision rim, and to firmly attach the metal plate to the head. After the surgical procedure, the animals were put in their cage on a pre-warmed heating pad to wake from anesthesia. They were provided with pre-wetted food pellets for easy chow and hydration. Postoperative care consisted of subcutaneous injections of Rimadyl (24 and 48 h post-surgery, dose as before). The convalescent animals were carefully monitored during the 7 days of post-surgery. When fully recovered from the surgery, habituation training began. The animals were gradually habituated to the experimenter, human handling, mobile homecage (Neurotar), head fixation, and imaging. Sugar water was used as a reward during training.

Pharmacology

DSP-4 (Tocris) was dissolved in saline, and a single dose of 75mg/kg body weight was administered >48 hours before imaging commenced.

Fluorescent dyes

All animals were injected through a venous catheter (acute experiments) or retroorbitally under isoflurane anesthesia (awake experiments) with a 2.5% weight/volume solution of Texas-Red dextran 70kDa in saline.

Two-photon imaging

All experiments were carried out on one of two imaging systems. The first microscope was a Leica SP5, DM6000 CFS multiphoton upright laser scanning microscope equipped with a MaiTai HP Ti:Sapphire laser (Millennia Pro, Spectra-Physics) using a 20x magnification and 1.0 numerical aperture water-immersion objective. Light emitted by the tissue was split by a dichromatic filter at 560 nm into two channels and collected by two separate multi-alkali photomultiplier tubes (PMTs) after 500-550 nm and 565-605 nm band-pass filtering (Leica Microsystems). The frame size for the Leica microscope was 256 x 256 pixels, representing a physical area of 129 µm2. Images were collected in a single plane by bidirectional scanning with a color depth of 16 bits. The total frame time for the microscope image capture corresponded to approximately 96 ms, with a sampling rate of around 10.38 Hz.

The second microscope was a commercial laser scanning multiphoton excitation system (FluoView FVMPE-RS, Olympus) paired with a Mai Tai HP Ti:Sapphire laser (Millenia Pro, Spectra-Physics) using a 25x magnification and 1.05 numerical aperture water-immersion objective (Olympus). In this microscope, the emitted light was split by a dichroic mirror with a 500-600 nm band-pass. Light reflected by the dichroic mirror was sent to a pair of gallium arsenide phosphide (GaAsP) PMTs, corresponding to the fluorescent signal from the vasculature. Light passing through the dichroic mirror was sent to a pair of multi-alkali PMTs, corresponding to the jGCaMP7f fluorescence from the neurons. Frame size was fixed at 512 x 512 pixels, representing a physical area of 127 µm2. Images were collected as a single plane by bidirectional scanning using a resonant scanner, reducing the color depth to 10 bits. The total frame time was also greatly reduced to 33 ms, corresponding to a sampling rate of 30 Hz.

Laser power was kept below 35 mW for all imaging to prevent phototoxicity. Laser emission was set to a wavelength of 920 nm for maximal excitation of the jGCaMP6f, jGCaMP7, and Texas Red fluorophores.

During imaging, the general behavior of the animal was recorded using a small standard video camera (Lifecam Studio, Microsoft), where the built-in IR filter had been removed and a long pass filter fitted (IR 930nm, Asahi Spectra). The LifeCam images were stored as uncompressed AVIs.

Whisker stimulation

Air puff whisker stimulation was delivered using a PV830 Pneumatic PicoPump from WPI. The air puff was directed towards the whiskers so that there was visible deflection without hitting anything else. The pressure was adjusted to the minimum level, which still resulted in visible deflections. The stimulation consisted of 100 ms pulses delivered at 3 Hz for 2 seconds.

Enlarged whisker deflection during natural whisking was accomplished by moving a small piece of sandpaper into the trajectory of the whiskers. This was done using a custom-built motorized arm controlled via an Arduino Uno.

Whisker tracking

An area-scan camera monitored the whisker pad and pupil triggered through the same circuit as the microscope, and a movement tracker was used (GO-5100M-PGE, JAI A/S, Denmark). Hence, images were synchronized with the 2-photon acquisition. This camera was fitted with a long-pass filter to only capture infrared light (930 nm, Asahi Spectra, Japan). JAI images were stored as uncompressed 8-bit BMP files. Both image series consisted only of greyscale images. Voluntary whisking events were detected by applying a Sobel filter to video recordings of the whiskers (Sup. Figure S1). The Sobel operator was applied to all images using Matlab's built-in imgradient function, and the two-dimensional intensity gradient was returned. The edges of the previous image were subtracted the edges of each image to determine if the edges detected had changed position. As the (i-1)'th frame was then subtracted from the i'th frame. The sum of the difference of all edges relative to its preceding frame was stored as the magnitude of whisker movement at that frame. The magnitudes of whisker movement were then thresholded at the median plus the standard deviation throughout the recording. Any frame above this threshold was labeled as "active whisking". If individual events occurred within half a second of one another, the events were grouped as one single event.

Pupil diameter detection

The JAI camera aimed at the whisker pad also allowed for accurate pupillometric measurements. A group of animals was studied separately from 2-photon imaging to ensure optimal lighting for accurate pupil

detection. We quantified the diameter changes using a custom-written ImageJ script (Supplemental Figure S8). First, the pupil was cropped, and the cropped image was denoised with a median filter. The background was uniformed using the Image Calculator feature. This involved combining the pixel intensities of two images: the inverted, Gaussian blurred image and the original image. After that, edges were detected using the "Find Edges" command, and the images were binarized using local thresholding methods (Mean, Niblack, Phansalkar). To address any gaps in objects (pupils) we employed "Open" and "Filll holes" commands. Lastly, the pupil was outlined using "Analyze Particles" command. Using Hull and circle plugin, Convex Hull area, diameter of the bounding circle, and other measurements of the outlined pupils were collected.

Movement tracking

Movement was tracked using the built-in sensor in the Neurotar Mobile Homecage system and the accompanying software (Locomotion Tracker Version 2.2.0.14, Neurotar, Finland). Movement tracking was saved as TDMS files and opened in Matlab. The listed acquisition speed was 80Hz, although a closer inspection of the timing intervals for each frame showed a hardware-level acquisition speed of approximately 77Hz. Displacement speed was thresholded at 1 cm/s to binarize locomotion.

Data analysis of two-photon images

All final image analysis was performed using Matlab. Simple, exploratory processing was done with ImageJ, LAS AF, or Olympus software. Leica microscopy files were initially evaluated and eventually exported using Leica's LAS AF software. The images were saved as TIFF images, and the metadata was saved in a separate XML document. Olympus microscopy files were opened, subtracted, and inspected with either ImageJ or Matlab, and all final analyses were performed in Matlab. To avoid data truncation, all image arithmetic performed on the original uint16 files was carried out as either 32- or 64-bit floating-point operations, single and double-precision, respectively.

Motion correction: All fluorescence recordings were motion-corrected before further analysis to remedy the slight disturbances introduced by mouse movement during imaging. Although the head-fixation set-up was quite stable and even allowed for imaging during periods of significant locomotion, all experiments benefitted from movement correction(Krogsgaard, Sperling et al. 2023). We corrected for movement within and between imaging sequences to maintain the exact field of view. Earlier movement correction was cross-correlation based, but we found normalized 2D cross-correlation corrected even finer movements. Our images possess features that could create false-positive cross-correlations, like

variable image and feature intensity. 2D cross-correlation slides a template over an image and calculates the similarity in intensity between the template and every portion of the image. Normalized cross-correlation subtracts the values of the template and the image region under the template by their respective means. This product is then divided by the standard deviations of both the template and the image region under the template. The normalization aims to ensure that image brightness does not create an artificially high correlation coefficient within the overly bright image segment. By using normalized cross-correlation, the edge strength of neuronal structures in mean intensity projections was improved even more when compared to standard cross-correlation.

Vasodilation: Vasodilations were calculated as dA/A. Penetrating arterioles and 1st order capillaries were manually selected and thresholded. Fluorescence videos of blood vessels were spatially smoothed using a 3 by 3 pixel median filter, preserving sharp edges while denoising with a Gaussian filter. Masks for vessels of interest were drawn by hand. All frames were thresholded using the triangle thresholding method. The binary images were cleaned up using morphological opening and closing, and the foreground area was calculated. The median of the whole trace was used as a baseline level to normalize dilation traces. The area was calculated and normalized by the median of the area trace for an entire recording. Using the triangle method, we thresholded and binarized the imaging sequence based on its intensity histogram. Morphological clean-up was performed, and the remaining binary area was taken to be the vessel area. This process was repeated for first-order capillaries as needed, with the only difference being the capillary ROI was manually outlined and applied as a polygon. Finally, the remaining binary areas were then used to determine the frame-by-frame change in area of the respective vessels and informed the perceived vasodilation and vasoconstriction. The median of the whole trace was used as the baseline level and would be the baseline by which to normalize the blood vessel trace.

Astrocytic dynamic ROIs:

Calcium microdomain detection: We developed a method that looked at changes in fluorescence and not the fluorescence strength. The method consisted of first thresholding, then cleanup of active voxels (two spatial dimensions and one temporal) – then clustering of detected active voxels – and then analysis of these clusters (Sup. Figure S3). The detection scheme outlined below is not too dissimilar to AQuA (Wang, DelRosso et al. 2019), although there are key differences. Thresholding was based on two parameters - the baseline (μ) estimated with the mode and the baseline variation (σ). A mode of the raw trace underestimates the baseline level as many pixels would often show no signal and, therefore, lie at the minimal fluorescence intensity value possible. Instead, we used the value around which the signal

fluctuates at rest. This value was found on smoothed data since, in this step, we are only interested in the level around which the signal fluctuates and not the fluctuations themselves. Hence, signals from each pixel were lowpass-filtered using a 5th order Butterworth filter with a cutoff frequency of 0.26 Hz (5% of the Nyquist rate)(Sup. Figure S3B). Then, the data was binned to width 50 counts, and the fluorescence signals were in the order of 10000s. This binning sacrifices some resolution to circumvent the issue of the minimal value appearing several times. By binning the signal, the value around which the signal fluctuates should be better represented to the single minimal value around which the signal does not fluctuate. After filtering and binning the mode was found to estimate the baseline level. An estimate for the baseline variation around the baseline level was found by high-passed filtering of the signals again using a Butterworth filter with the same cutoff frequency as the lowpass filter. By doing this, we discard the larger changes stemming from actual calcium activity within the cell and just get the high frequency of noise through which the signals must stand out to be detected. As a first rough estimate of the baseline variation, we take the standard deviation of this high-pass filtered trace. Finding the variance using the standard deviation of this signal will be an overestimate, as the fluorescence noise is partly due to Poisson processes in the fluorophores and in the detectors. For the Poisson distribution, the variance is equal to the mean ($\mu = \sigma 2$), so with more signal strength, we get larger variation as well. Thus, we used a variance stabilization strategy based on iterations. To find the baseline, we threshold the signal with our current estimates (the baseline level is found as described above, and the baseline variation is represented by the standard deviation of the high pass filtered signal).

Anything below a threshold of $\mu i + 2 \cdot \sigma i$ the i'th pixel) is considered to belong to the true baseline. We then used this new trace, where we discarded a large portion of the calcium signals, to better estimate the baseline level and variation (Sup. Figure S1D). We then used this estimation of baseline level and variation to threshold each pixel signal (Sup. Figure S1E). Next was a clean-up of the detected active voxels. Even after a threshold at two sigma, there will still be some false positives; thus, lone voxels without any active neighbors were disregarded, and voxels that were close together were grouped. Since the data is a binary 3D set (spatiotemporal, Sup. Figure S1F), this can be accomplished by using simple morphological operations known as opening and closing, commonly used for noise removal in computer vision (Sup. Figure 1G).

The next step clusters the active voxels into domains that are active together. Clustering was done in 2D, but to avoid clustering events that might partially or wholly be within the same spatial region but do not overlap in time, the binary 3D array was first projected into 2D. The overlapping clusters were thus

projected onto the same or connected pixels and consequently clustered together. This may result in underestimation of the amplitude of spatially small signals that happen to lie within a larger cluster as the average fluorescence of the whole area is calculated for each frame. If only part of the cluster is active in some frames, this will lead to underestimation of that signal.

This metric yields the total area of the FOV, which was active at some point during the recording, the total integrated fluorescence of all signals within the recording, and the number of spatial regions where the activity took place. ΔF/F-traces from these clusters can be further worked upon (Sup. Figure S1I). The accuracy of this detection algorithm was tested on synthetic data produced at various levels of contrast and signal-to-noise ratio (SNR).

Astrocytic context-dependent ROIs:

To identify regions of astrocyte activity in relation to NVC processes, we first detected dilation peaks in the PA area trace (Sup. Figure S5). Dilation events preceded by whisking but did not overlap with locomotion or air-puff stimulation were selected. Only periods with at least 2 seconds of baseline prior to the dilation peak were included. The average fluorescence levels in a 1 second period from 2-1 second before the dilation peak was averaged. From this, a mask was created by applying a 2D Gaussian filter (imgaussfilt.mat) to denoise and threshold the ROIs. Using the bwareafilt.mat function areas smaller than 1.5μm^2 pixels were excluded. The filtered image was binarized to create a mask. In this image, we identified regions with maximal activity in the astrocytic Ca2+ levels one second before the dilation peak. These ROIs were then grouped depending on the distance from the PA. The innermost 15µm ring from the center of the PA was excluded to eliminate any disturbances from the changes in vessel diameter. That also meant that end-feet structures were not investigated in this study. The data was then grouped into four zones counting from the outer rim of the innermost circle: <15µm from PA, 15-30µm from PA, 30-45µm and 45-60µm from PA. The average activity in these ROIs was then measured for each image in the acquisition in the entire imaging session.

Neuronal ROI placement:

These ROIs were selected based on the maximum projection of several frames at intervals to whisking onset and application of a 2D Gaussian filter to denoise and threshold the ROIs. An additional intensity thresholding step and morphological operations excluded excessively small and low-intensity ROIs. Furthermore, algorithmically determined and manually corrected soma were superimposed as outlines

to demonstrate whether our unbiased ROIs reflected structural compartments. Activity in these ROIs could then be compared between stimuli and pharmacological conditions.

To find the regions most active during whisking, we created average images of the periods surrounding whisking. We began with sorting whisking events and creating ΔF/F calcium images. First, all whisking events were labeled as overlapping with movement or not, and all overlapping with movement were discarded. Next, all whisking events that began within the first .2 seconds of recording were discarded. Finally, all whisking events with durations shorter than one second and longer than three seconds were discarded. Based on previous data within the group, we selected this 1-3 second window as most relevant to the hemodynamic response to whisking. To calculate ΔF/F values, we first selected the baseline calcium signal for each imaging sequence. We identified the calcium images corresponding to periods without any whisking or movement and averaged these images. We then subtracted and divided all images in the sequence by this baseline, converting all images in the sequence into ΔF/F values. For the remaining one- to three-second-long whisking events, the calcium images corresponding to seven seconds before and after each whisking onset were summed together to form 14-second-long cropped average calcium images, which were in each case centered on the onset of the whisking episode.

Having created whisking-aligned composite images, we had to define which period was relevant to whisking activity. We used a 500 millisecond (ms) window, 100 ms before and 400 ms after whisking onset. We normalized our composite ΔF/F images on their per-pixel distributions. We used the periods prior to whisking onset with less than 50% whisking activity as a baseline and subtracted the per-pixel baseline from all images. We then calculated the standard deviation of each pixel over the entire 14-second period and divided each pixel by its standard deviation. From these normalized images, we could identify the most active regions in the half-second around whisking. We selected our ROIs according to the morphology and size of these active regions, which we further classified into relevant neuronal subcompartments.

Our next goal was to parse the neuronal calcium response to natural whisking. We generated a series of average images aligned to the onest of the whisking events. Before selecting areas associated with whisking, we excluded whisking events with movement and air puff stimulation. We selected the 120 most active regions, as indicated by their respective normalized values. Next, these regions were automatically grouped into three categories according to size and shape: soma, dendrite, and synapse. Soma and distinct neuropil could be seen, although we could not determine whether these processes were axonal or dendritic, so we decided to err towards labeling them dendritic. We also noticed small

active areas without clear compartmental identities and, depending on size, labeled them as dendritic or synaptic. These automatic morphological groupings were then manually checked and recategorized as necessary by comparing them to manually outlined soma maps and field-of-view intensity projections. Having selected the whisking relevant areas, we added two final ROIs to capture the background calcium response. The first was the fluorescence of the entire field of view (FOV). The second captured the less active areas, labeled "neuropil" (NP). By creating an aggregate mask of all morphological ROIs, slightly expanding their areas, and applying it to the respective imaging sessions, we could exclude the whisking-activated areas and select a lower activity field of view. We extracted traces for each imaging sequence from each ROI, three morphological and two fields-of-view: soma, dendrite, synapse, and NP, FoV. This entire process was repeated for each imaging session separately due to slight variations in our z-plane between imaging days. Although this z-plane change was minor, even a few microns can determine whether a neuronal process is within our imaging plane.

Statistics

To compare the anticipatory and reactive responses of our stimuli, sandpaper, and air puff, to their respective controls, we classified whisking activity into four different categories: volitional whisking at rest with and without sandpaper, air puff evoked whisking events and whisking events that overlapped with locomotion events of >2 seconds duration. The analysis did not include whisking that overlapped with locomotion shorter than 2 seconds. For comparison between volitional whisking events during rest, with or without sandpaper, only event lasting between 1 to 3 seconds was included. When comparing to the 2-second duration air-puff, only volitional whisking events lasting 1.5 to 2.5 seconds were included. When comparing volitional whisking events during rest to those during locomotion, only events >2 seconds were included. Responses to separate whisking events were averaged according to the FOV from which the measurement was made. N=20 FOV from 16 mice was included in the investigation of the blood vessel and astrocyte CA2+ activity investigation. N=19 FOVs from 8 mice were included in the study of neuronal Ca2+ activity. These averages were used for statistical testing, as they were considered the relevant entity. Namely, this specific PA, 1st order capillary, astrocytic or neuronal structure. The baseline was calculated per event as each whisking event was individually normalized to the activity directly preceding it. The trace one to eight seconds before each whisking onset was taken as a baseline for each whisking event. Periods within two seconds of movement were omitted. For air puff trials, we found the limited number of trials made the traces and respective baselines more susceptible to excessive animal movement. We shortened the baseline period to one to four seconds before stimulus

onset to address this. This reduced trace variance before and after stimulus onset. Statistical tests were either one-sample, two-sided t-tests, paired t-tests, or Wilcoxon tests. One-sample t-tests were used to compare traces to the baseline. Paired t-tests were used when comparing stimuli to their controls: sandpaper against free whisking and air puff against 2-second whisking events. Wilcoxon test was used when comparing time-locked or counted data as these could not be expected to show normal distribution. Normality was tested visually with a qq-plot, and data were log-transformed when appropriate. Mixed effects models were used to test significance followed by two-tailed paired or unpaired Student's t-test as appropriate with Holm-Sidak correction for multiple comparisons. Significance was set at a level of 0.05. Single stars indicate p-values < 0.05, two stars < 0.01, and three stars < 0.001.

Acknowledgment

We would like to acknowledge our animal technician, Micael Lønstrup, for his help with animal experiments. Thanks to Dr. Kirsten Thomsen for statistical advice and guidance. Professor MD Anna Devor and her laboratory for training experiments on awake mice. Professor Martin Lauritzen and associate professor Krzysztof Kucharz for good advice. This study was supported by "Læge Sofus Carl Emil Friis og Hustru Olga Doris Friis' Legat", "Dagmar Marshalls Fond," and "Hørslev fonden".

Author's contribution

A.K. and B.L. designed the study. A.K., J.S., G.K., L.S., and B.L. performed the experiments. A.K., J.S., G.K., and B.L. analyzed the data. B.L., A.K., and J.S. wrote the paper with input from all authors.

Declaration of interest

The authors declare no conflicts of interest.

Data availability

The data supporting these findings are available from the corresponding author upon reasonable request.

Code availability

Code is available from the corresponding author upon reasonable request.

Supplemental material

See below.

References

Arizono, M., V. V. G. K. Inavalli, A. Panatier, T. Pfeiffer, J. Angibaud, F. Levet, M. J. T. Ter Veer, J. Stobart, L. Bellocchio, K. Mikoshiba, G. Marsicano, B. Weber, S. H. R. Oliet and U. V. Nägerl (2020). "Structural basis of astrocytic Ca2+ signals at tripartite synapses." Nature Communications **11**(1): 1906.

Armbruster, M., S. Naskar, J. P. Garcia, M. Sommer, E. Kim, Y. Adam, P. G. Haydon, E. S. Boyden, A. E. Cohen and C. G. Dulla (2022). "Neuronal activity drives pathway-specific depolarization of peripheral astrocyte processes." Nat Neurosci **25**(5): 607-616.

Biesecker, K. R. and A. I. Srienc (2015). "The functional role of astrocyte calcium signaling in cortical blood flow regulation." J Neurosci **35**(3): 868-870.

Biesecker, K. R., A. I. Srienc, A. M. Shimoda, A. Agarwal, D. E. Bergles, P. Kofuji and E. A. Newman (2016). "Glial Cell Calcium Signaling Mediates Capillary Regulation of Blood Flow in the Retina." J Neurosci **36**(36): 9435-9445.

Bindocci, E., I. Savtchouk, N. Liaudet, D. Becker, G. Carriero and A. Volterra (2017). "Three-dimensional Ca2+ imaging advances understanding of astrocyte biology." Science **356**(6339).

Bojarskaite, L., D. M. Bjornstad, K. H. Pettersen, C. Cunen, G. H. Hermansen, K. S. Abjorsbraten, A. R. Chambers, R. Sprengel, K. Vervaeke, W. Tang, R. Enger and E. A. Nagelhus (2020). "Astrocytic Ca(2+) signaling is reduced during sleep and is involved in the regulation of slow wave sleep." Nat Commun **11**(1): 3240.

Bonder, D. E. and K. D. McCarthy (2014). "Astrocytic Gq-GPCR-linked IP3R-dependent Ca2+ signaling does not mediate neurovascular coupling in mouse visual cortex in vivo." J Neurosci **34**(39): 13139-13150.

Cerpa, J. C., A. Piccin, M. Dehove, M. Lavigne, E. J. Kremer, M. Wolff, S. L. Parkes and E. Coutureau (2023). "Inhibition of noradrenergic signalling in rodent orbitofrontal cortex impairs the updating of goal-directed actions." Elife **12**.

Collins, L., J. Francis, B. Emanuel and D. A. McCormick (2023). "Cholinergic and noradrenergic axonal activity contains a behavioral-state signal that is coordinated across the dorsal cortex." Elife **12**.

Del Franco, A. P., P. P. Chiang and E. A. Newman (2022). "Dilation of cortical capillaries is not related to astrocyte calcium signaling." Glia **70**(3): 508-521.

Devilbiss, D. M. (2019). "Consequences of tuning network function by tonic and phasic locus coeruleus output and stress: Regulating detection and discrimination of peripheral stimuli." Brain Res **1709**: 16-27.

Devor, A., I. Ulbert, A. K. Dunn, S. N. Narayanan, S. R. Jones, M. L. Andermann, D. A. Boas and A. M. Dale (2005). "Coupling of the cortical hemodynamic response to cortical and thalamic neuronal activity." Proceedings of the National Academy of Sciences of the United States of America **102**(10): 3822-3827.

Ding, F., J. O'Donnell, A. S. Thrane, D. Zeppenfeld, H. Kang, L. Xie, F. Wang and M. Nedergaard (2013). "alpha1-Adrenergic receptors mediate coordinated Ca2+ signaling of cortical astrocytes in awake, behaving mice." Cell Calcium **54**(6): 387-394.

Drew, P. J. (2022). "Neurovascular coupling: motive unknown." Trends Neurosci **45**(11): 809-819.

Eyre, B., K. Shaw, P. Sharp, L. Boorman, L. Lee, O. Shabir, J. Berwick and C. Howarth (2022). "The effects of locomotion on sensory-evoked haemodynamic responses in the cortex of awake mice." Sci Rep **12**(1): 6236.

Girouard, H., A. D. Bonev, R. M. Hannah, A. Meredith, R. W. Aldrich and M. T. Nelson (2010). "Astrocytic endfoot Ca2+ and BK channels determine both arteriolar dilation and constriction." Proc.Natl.Acad.Sci.U.S.A **107**(8): 3811-3816.

Gordon, G. R., H. B. Choi, R. L. Rungta, G. C. Ellis-Davies and B. A. MacVicar (2008). "Brain metabolism dictates the polarity of astrocyte control over arterioles." Nature **456**(7223): 745-749.
Grubb, S., C. Cai, B. O. Hald, L. Khennouf, R. P. Murmu, A. G. K. Jensen, J. Fordsmann, S. Zambach and M. Lauritzen (2020). "Precapillary sphincters maintain perfusion in the cerebral cortex." Nat Commun **11**(1): 395.
Gu, X., W. Chen, N. D. Volkow, A. P. Koretsky, C. Du and Y. Pan (2018). "Synchronized Astrocytic Ca(2+) Responses in Neurovascular Coupling during Somatosensory Stimulation and for the Resting State." Cell Rep **23**(13): 3878-3890.
Hartmann, D. A., V. Coelho-Santos and A. Y. Shih (2022). "Pericyte Control of Blood Flow Across Microvascular Zones in the Central Nervous System." Annu Rev Physiol **84**: 331-354.
Howarth, C., A. Mishra and C. N. Hall (2021). "More than just summed neuronal activity: how multiple cell types shape the BOLD response." Philos Trans R Soc Lond B Biol Sci **376**(1815): 20190630.
Iannitelli, A. F., M. A. Kelberman, D. J. Lustberg, A. Korukonda, K. E. McCann, B. Mulvey, A. Segal, L. C. Liles, S. A. Sloan, J. D. Dougherty and D. Weinshenker (2023). "The Neurotoxin DSP-4 Dysregulates the Locus Coeruleus-Norepinephrine System and Recapitulates Molecular and Behavioral Aspects of Prodromal Neurodegenerative Disease." eNeuro **10**(1).
Institoris, A., D. G. Rosenegger and G. R. Gordon (2015). "Arteriole dilation to synaptic activation that is sub-threshold to astrocyte endfoot Ca transients." J Cereb Blood Flow Metab.
Institoris, A., M. Vandal, G. Peringod, C. Catalano, C. H. Tran, X. Yu, F. Visser, C. Breiteneder, L. Molina, B. S. Khakh, M. D. Nguyen, R. J. Thompson and G. R. Gordon (2022). "Astrocytes amplify neurovascular coupling to sustained activation of neocortex in awake mice." Nat Commun **13**(1): 7872.
Jessen, S. B., C. Mathiesen, B. L. Lind and M. Lauritzen (2017). "Interneuron Deficit Associates Attenuated Network Synchronization to Mismatch of Energy Supply and Demand in Aging Mouse Brains." Cereb Cortex **27**(1): 646-659.
Kim, J. H., A. H. Jung, D. Jeong, I. Choi, K. Kim, S. Shin, S. J. Kim and S. H. Lee (2016). "Selectivity of Neuromodulatory Projections from the Basal Forebrain and Locus Ceruleus to Primary Sensory Cortices." J Neurosci **36**(19): 5314-5327.
Kinnischtzke, A. K., D. J. Simons and E. E. Fanselow (2014). "Motor cortex broadly engages excitatory and inhibitory neurons in somatosensory barrel cortex." Cereb Cortex **24**(8): 2237-2248.
Krogsgaard, A., L. Sperling, M. Dahlqvist, K. Thomsen, G. Vydmantaite, F. Li, M. Thunemann, M. Lauritzen and B. L. Lind (2023). "PV interneurons evoke astrocytic Ca(2+) responses in awake mice, which contributes to neurovascular coupling." Glia **71**(8): 1830-1846.
Lacroix, A., X. Toussay, E. Anenberg, C. Lecrux, N. Ferreiros, A. Karagiannis, F. Plaisier, P. Chausson, F. Jarlier, S. A. Burgess, E. M. Hillman, I. Tegeder, T. H. Murphy, E. Hamel and B. Cauli (2015). "COX-2-Derived Prostaglandin E2 Produced by Pyramidal Neurons Contributes to Neurovascular Coupling in the Rodent Cerebral Cortex." J Neurosci **35**(34): 11791-11810.
Lecrux, C., C. H. Sandoe, S. Neupane, P. Kropf, X. Toussay, X. K. Tong, M. Lacalle-Aurioles, A. Shmuel and E. Hamel (2017). "Impact of Altered Cholinergic Tones on the Neurovascular Coupling Response to Whisker Stimulation." J Neurosci **37**(6): 1518-1531.
Lind, B. L., A. R. Brazhe, S. B. Jessen, F. C. Tan and M. J. Lauritzen (2013). "Rapid stimulus-evoked astrocyte Ca2+ elevations and hemodynamic responses in mouse somatosensory cortex in vivo." Proc Natl Acad Sci U S A **110**(48): E4678-4687.
Lind, B. L., S. B. Jessen, M. Lonstrup, C. Josephine, G. Bonvento and M. Lauritzen (2018). "Fast Ca(2+) responses in astrocyte end-feet and neurovascular coupling in mice." Glia **66**(2): 348-358.
Masamoto, K., M. Unekawa, T. Watanabe, H. Toriumi, H. Takuwa, H. Kawaguchi, I. Kanno, K. Matsui, K. F. Tanaka, Y. Tomita and N. Suzuki (2015). "Unveiling astrocytic control of cerebral blood flow with optogenetics." Sci Rep **5**: 11455.

Mathiisen, T. M., K. P. Lehre, N. C. Danbolt and O. P. Ottersen (2010). "The perivascular astroglial sheath provides a complete covering of the brain microvessels: an electron microscopic 3D reconstruction." Glia **58**(9): 1094-1103.
McCaslin, A. F., B. R. Chen, A. J. Radosevich, B. Cauli and E. M. Hillman (2011). "In vivo 3D morphology of astrocyte-vasculature interactions in the somatosensory cortex: implications for neurovascular coupling." J Cereb Blood Flow Metab **31**(3): 795-806.
Metea, M. R. and E. A. Newman (2006). "Glial cells dilate and constrict blood vessels: a mechanism of neurovascular coupling." J Neurosci **26**(11): 2862-2870.
Mishra, A., F. M. O'Farrell, C. Reynell, N. B. Hamilton, C. N. Hall and D. Attwell (2014). "Imaging pericytes and capillary diameter in brain slices and isolated retinae." Nat Protoc **9**(2): 323-336.
Mishra, A., J. P. Reynolds, Y. Chen, A. V. Gourine, D. A. Rusakov and D. Attwell (2016). "Astrocytes mediate neurovascular signaling to capillary pericytes but not to arterioles." Nat Neurosci **19**(12): 1619-1627.
Montalant, A., O. Kiehn and J. F. Perrier (2024). "Dopamine and noradrenaline activate spinal astrocyte endfeet via D1-like receptors." Eur J Neurosci **59**(6): 1278-1295.
Mulligan, S. J. and B. A. MacVicar (2004). "Calcium transients in astrocyte endfeet cause cerebrovascular constrictions 1." Nature **431**(7005): 195-199.
Nizar, K., H. Uhlirova, P. Tian, P. A. Saisan, Q. Cheng, L. Reznichenko, K. L. Weldy, T. C. Steed, V. B. Sridhar, C. L. MacDonald, J. Cui, S. L. Gratiy, S. Sakadžić, D. A. Boas, T. I. Beka, G. T. Einevoll, J. Chen, E. Masliah, A. M. Dale, G. A. Silva and A. Devor (2013). "In vivo Stimulus-Induced Vasodilation Occurs without IP3 Receptor Activation and May Precede Astrocytic Calcium Increase." The Journal of Neuroscience **33**(19): 8411-8422.
Oe, Y., X. Wang, T. Patriarchi, A. Konno, K. Ozawa, K. Yahagi, H. Hirai, T. Tsuboi, T. Kitaguchi, L. Tian, T. J. McHugh and H. Hirase (2020). "Distinct temporal integration of noradrenaline signaling by astrocytic second messengers during vigilance." Nat Commun **11**(1): 471.
Otsu, Y., K. Couchman, D. G. Lyons, M. Collot, A. Agarwal, J. M. Mallet, F. W. Pfrieger, D. E. Bergles and S. Charpak (2015). "Calcium dynamics in astrocyte processes during neurovascular coupling." Nat Neurosci **18**(2): 210-218.
Paukert, M., A. Agarwal, J. Cha, V. A. Doze, J. U. Kang and D. E. Bergles (2014). "Norepinephrine controls astroglial responsiveness to local circuit activity." Neuron **82**(6): 1263-1270.
Petersen, C. C. H. (2019). "Sensorimotor processing in the rodent barrel cortex." Nat Rev Neurosci **20**(9): 533-546.
Petzold, G. C., D. F. Albeanu, T. F. Sato and V. N. Murthy (2008). "Coupling of neural activity to blood flow in olfactory glomeruli is mediated by astrocytic pathways." Neuron **58**(6): 897-910.
Poulet, J. F. A. and S. Crochet (2018). "The Cortical States of Wakefulness." Front Syst Neurosci **12**: 64.
Reitman, M. E., V. Tse, X. Mi, D. D. Willoughby, A. Peinado, A. Aivazidis, B. E. Myagmar, P. C. Simpson, O. A. Bayraktar, G. Yu and K. E. Poskanzer (2023). "Norepinephrine links astrocytic activity to regulation of cortical state." Nat Neurosci **26**(4): 579-593.
Renden, R. B., A. Institoris, K. Sharma and C. H. T. Tran (2024). "Modulatory effects of noradrenergic and serotonergic signaling pathway on neurovascular coupling." Commun Biol **7**(1): 287.
Roy, C. and C. Sherrington (1890). "On the regulation of the blood supply of the brain." J.Physiol.Lond. **11**: 85-108.
Santello, M., N. Toni and A. Volterra (2019). "Astrocyte function from information processing to cognition and cognitive impairment." Nature Neuroscience **22**(2): 154-166.
Schaeffer, S. and C. Iadecola (2021). "Revisiting the neurovascular unit." Nat Neurosci **24**(9): 1198-1209.
Sharma, K., G. R. J. Gordon and C. H. T. Tran (2020). "Heterogeneity of Sensory-Induced Astrocytic Ca(2+) Dynamics During Functional Hyperemia." Front Physiol **11**: 611884.
Shigetomi, E., E. A. Bushong, M. D. Haustein, X. Tong, O. Jackson-Weaver, S. Kracun, J. Xu, M. V. Sofroniew, M. H. Ellisman and B. S. Khakh (2013). "Imaging calcium microdomains within entire astrocyte

territories and endfeet with GCaMPs expressed using adeno-associated viruses." J Gen Physiol **141**(5): 633-647.
Shimaoka, D., K. D. Harris and M. Carandini (2018). "Effects of Arousal on Mouse Sensory Cortex Depend on Modality." Cell Rep **25**(11): 3230.
Slezak, M., S. Kandler, P. P. Van Veldhoven, C. Van den Haute, V. Bonin and M. G. Holt (2019). "Distinct Mechanisms for Visual and Motor-Related Astrocyte Responses in Mouse Visual Cortex." Curr Biol **29**(18): 3120-3127 e3125.
Sofroniew, N. J., J. D. Cohen, A. K. Lee and K. Svoboda (2014). "Natural whisker-guided behavior by head-fixed mice in tactile virtual reality." J Neurosci **34**(29): 9537-9550.
Stobart, J. L., K. D. Ferrari, M. J. P. Barrett, C. Gluck, M. J. Stobart, M. Zuend and B. Weber (2018). "Cortical Circuit Activity Evokes Rapid Astrocyte Calcium Signals on a Similar Timescale to Neurons." Neuron **98**(4): 726-735 e724.
Takano, T., G. F. Tian, W. G. Peng, N. H. Lou, W. Libionka, X. N. Han and M. Nedergaard (2006). "Astrocyte-mediated control of cerebral blood flow." Nature Neuroscience **9**(2): 260-267.
Thrane, A. S., V. R. Thrane, D. Zeppenfeld, N. Lou, Q. Xu, E. A. Nagelhus and M. Nedergaard (2012). "General anesthesia selectively disrupts astrocyte calcium signaling in the awake mouse cortex." Proc Natl Acad Sci U S A **109**(46): 18974-18979.
Toussay, X., K. Basu, B. Lacoste and E. Hamel (2013). "Locus coeruleus stimulation recruits a broad cortical neuronal network and increases cortical perfusion." J Neurosci **33**(8): 3390-3401.
Tran, C. H. T., G. Peringod and G. R. Gordon (2018). "Astrocytes Integrate Behavioral State and Vascular Signals during Functional Hyperemia." Neuron **100**(5): 1133-1148 e1133.
Turner, K. L., K. W. Gheres and P. J. Drew (2023). "Relating Pupil Diameter and Blinking to Cortical Activity and Hemodynamics across Arousal States." J Neurosci **43**(6): 949-964.
Wang, J., Y. Jang, J. K. Khedkar, J. Y. Koo, Y. Kim, C. J. Lee, Y. M. Rhee and K. Kim (2016). "How Does Solvation Affect the Binding of Hydrophilic Amino Saccharides to Cucurbit[7]uril with Exceptional Anomeric Selectivity?" Chemistry **22**(44): 15791-15799.
Wang, X., N. Lou, Q. Xu, G. F. Tian, W. G. Peng, X. Han, J. Kang, T. Takano and M. Nedergaard (2006). "Astrocytic Ca2+ signaling evoked by sensory stimulation in vivo." Nat Neurosci **9**(6): 816-823.
Wang, Y., N. V. DelRosso, T. V. Vaidyanathan, M. K. Cahill, M. E. Reitman, S. Pittolo, X. Mi, G. Yu and K. E. Poskanzer (2019). "Accurate quantification of astrocyte and neurotransmitter fluorescence dynamics for single-cell and population-level physiology." Nat Neurosci **22**(11): 1936-1944.
Winder, A. T., C. Echagarruga, Q. Zhang and P. J. Drew (2017). "Weak correlations between hemodynamic signals and ongoing neural activity during the resting state." Nat Neurosci **20**(12): 1761-1769.
Winship, I. R., N. Plaa and T. H. Murphy (2007). "Rapid astrocyte calcium signals correlate with neuronal activity and onset of the hemodynamic response in vivo." J.Neurosci. **27**(23): 6268-6272.